HETEK

Control of Early Age Cracking in Concrete Phase 2: Shrinkage of Mortar and Concrete

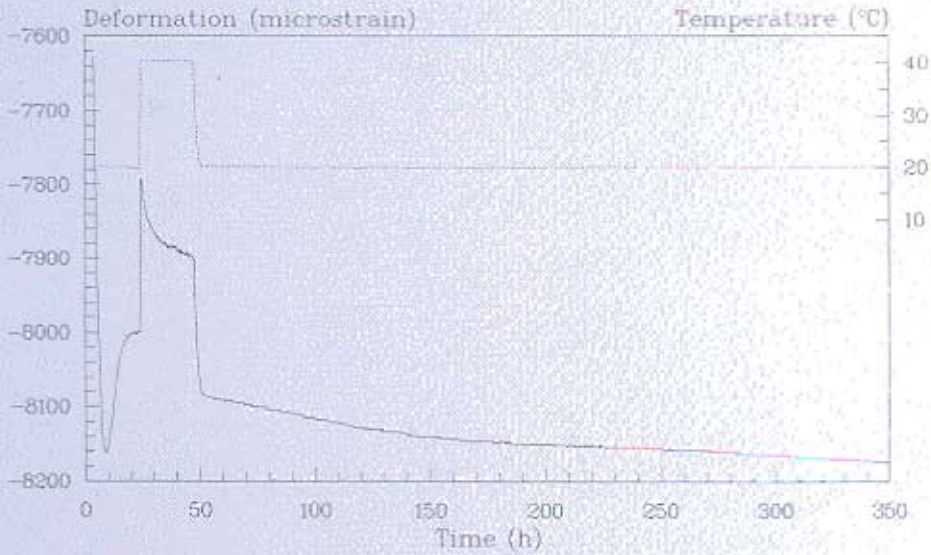

Report No.110
1997

Road Directorate Denmark Ministry of Transport

IRRD Information

Title in English	**HETEK -Control of Early Age Cracking in Concrete - Phase 2: Shrinkage of mortar and concrete**
Title in Danish	**HETEK -Styring af revner i ung beton - Fase 2: Svind af mørtel og beton**
Authors	Ole Mejlhede Jensen, Søren Lolk Christensen, Birgitte Friis Dela, Jacob Hougaard Hansen, Per Freiesleben Hansen, Anders Nielsen
Subject classification	Field 32 Concrete

Key words		
	Concrete	4755
	Analysis	7152
	Material (constr)	4555
	Numerical	6432
	Properties	5925
	Thermal stress in material	5575
	Denmark	8028

Abstract

This report deals with autogenous shrinkage of two concretes and the corresponding mortars. The theory of self-desiccation and autogenous deformation is presented. Autogenous shrinkage of mortar is measured in a paste dialtometer at constant and varying temperatures. Similarly the autogenous shrinkage of the concrete is measured in a concrete dilatometer developed in this project. The results are discussed in relation to thermal expansion, activation energy and maturity transformation.

UDK	691.32 620.191.33
ISSN	0909-4288
ISBN	87-7491-8230

Contents

0 Preface

This project on control of early age cracking is part of the Danish Road Directorate's research programme, High Performance Concrete - The Contractor's Technology, abbreviated to HETEK.

In this programme high performance concrete is defined as concrete with a service life in excess of 100 years in an aggressive environment.

The research programme includes investigations concerning the contractor's design of high performance concrete and execution of the concrete work with reference to the required service life of 100 years.

The total HETEK research programme is divided into segments parts with the following topics:

- chloride penetration
- frost resistance
- control of early-age cracking
- curing (evaporation protection)
- trial casting
- repair of defects.

The Danish Road Directorate invited tenders for this research programme which is mainly financed by the Danish Ministry for Commerce and Industry - The Commision of Research and Development Contracts.

The present report refers to the part of the HETEK project which deals with control of early age cracking.

For durability reasons reinforced structural members should be well protected against penetration of water, chloride etc. This means that cracks should be avoided or at least the crack-width limited. Formation of cracks can take place already during the hardening process. An evaluation of the risk of crack formation involves a stress analysis. In stress analysis of hardening concrete structures, the load consists of the autogenous deformation and the differences in thermal strains that arise from the heat of hydration. The mechanical properties also change during the hardening process. If a stress analysis shows high stresses compared to the tensile strength there is a high risk of crack formation.

The purpose of this project is to investigate these effects and to prepare a guideline regarding Control of Early Age Cracking.

The project was carried out by a consortium consisting of:

Danish Concrete Institute represented by:

Højgaard & Schultz A/S
Monberg & Thorsen A/S
RAMBØLL
COWI

and

Danish Technological Institute, represented by the Concrete Centre

and

Technical University of Denmark, represented by the Department of Strucutral Engineering and Materials.

Two external consultants, professor Per Freiesleben Hansen and manager Jens Frandsen, are connected with the consortium.

The present report on Shrinkage of mortar and concrete has been carried out at the Technical University of Denmark. Chapter 2, 3 and 4 of this report is mainly based on Ole Mejlhede Jensen[1].

1 Introduction

In order to avoid durability problems in reinforced concrete structures it is necessary to limit the formation of cracks during the hardening period. Cracks can of course be caused by external loads, settlements, etc., but there is also a risk of crack formation during the hardening process. The main cause of cracks in this period is thermal strain arising from the heat development of the concrete. Thermal strains have traditionally been limited by requiring the contractor to plan the concrete work so that large temperature differences between different parts of the structure do not arise.

Strains arising from shrinkage play a secondary but significant part in the concretes normally used in Denmark. The shrinkage can be divided into two parts: shrinkage arising from evaporation and autogenous shrinkage. The strains arising from autogenous shrinkage cannot be influenced by the contractor except through the choice of concrete mix design, but shrinkage arising from evaporation can be acoided by making an appropriate evaporation protection.

The present report deals with strains originating from autogenous shrinkage.

2 Terminology

The terminology associated with the field of cement technology that this report deals with is not well established. Different terms are used for the same phenomenon and different phenomena are described by the same term. This confusion of nomenclature exists in several languages. As an example the unrestrained bulk deformation of sealed cement paste at a constant temperature has been called: chemical shrinkage[12], bulk chemical shrinkage[9], chemical volume change[21], self-desiccation shrinkage[52], autogenous deformation[23], autogenous shrinkage[70], autogenous volume change[21], endogenous shrinkage[148] and indigenous shrinkage[16]. The terms used in this report are described as follows:

Chemical shrinkage: Internal volume reduction associated with the hydration of Portland cement, i.e. the volume of the hydrates is less than the volume of the oxides and water reacted.

In a closed isothermal system chemical shrinkage may cause a lowering of the chemical potential of the pore water, either by formation of menisci or by changing the equilibrium state of the adsorbed pore water. In either case this will affect the internal relative humidity (RH) and cause a dimensional change of the system. On this basis the following terminology is defined for an unrestrained hardening cement paste system, cf. Figure 1:

Autogenous deformation: Bulk deformation of a closed isothermal cement paste system.

Self-desiccation shrinkage: Bulk shrinkage of a closed isothermal cement paste system caused by chemical shrinkage.

Autogenous RH-change: Change of the internal relative humidity in a closed isothermal cement paste system.

Self-desiccation: Lowering of the internal relative humidity in a closed isothermal cement paste system caused by chemical shrinkage.

The internal relative humidity in a cement paste is the relative humidity with which the pore water is in equilibrium. The internal relative humidity is thus an indicator of the activity of the pore water.

Autogenous deformation and autogenous RH-change are active in open cement paste systems as well. In that case the autogenous phenomena are merely superposed and modified by the external influence.

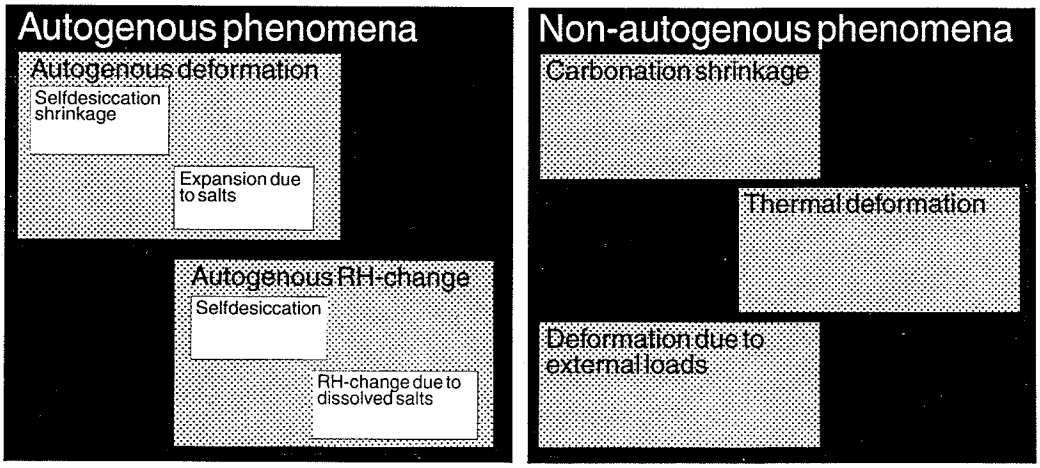

Figure 1. Graphic representation of the applied terminology. Self-desiccation and self-desiccation shrinkage are proper subsets of autogenous RH-change and autogenous deformation respectively.

3 Theory

3.1 Self-desiccation and self-desiccation shrinkage

Self-desiccation and self-desiccation shrinkage are caused by chemical shrinkage accompanying the cement hydration. It is well-known that the hydration products formed by Portland cement hydration occupy less space than the reacting water and cement. After setting this phenomenon, chemical shrinkage, results in inner gas-filled cavities if the cement paste is kept sealed. As hydration proceeds, smaller and smaller pores will successively be emptied. Through the formation of menisci, this process leads to a decrease of the relative humidity within the pores, i.e. self-desiccation, and due to tensile stresses in the pore water the cement paste shrinks - i.e. self-desiccation shrinkage.

In this way chemical shrinkage simultaneously leads to self-desiccation and self-desiccation shrinkage; that means self-desiccation shrinkage should not be regarded as a result of self-desiccation. The self-desiccation and self-desiccation shrinkage produced by the chemical shrinkage closely resemble the desiccation and desiccation shrinkage that result from loss of water to the surroundings.

The above description of self-desiccation and self-desiccation shrinkage is supported experimentally by Buil[26] and Hua et al.[18]. Figure 2 illustrates the described consequences of cement hydration:

- Reduction of the amount of pore water due to chemical binding in the hydration products
- Growth of the solid phase and refinement of the pore structure
- Formation of gas-filled voids due to chemical shrinkage
- Reduction of the radius of curvature of the menisci.

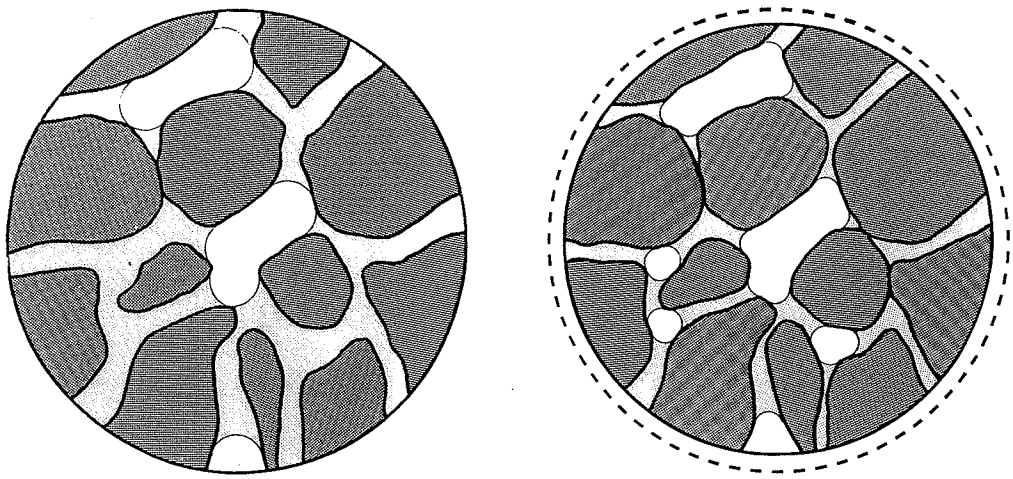

Figure 2. Simplified illustration of a cross-section in a self-desiccating cement paste. Left: low degree of hydration. Right: high degree of hydration. The phases shown are: solid (dark grey), pore water (light grey) and gas-filled voids.

3.2 Autogenous RH-change

3.2.1 Self-desiccation according to Powers' model

Based on several years research, a model for the phase distribution in hardening Portland cement paste was presented by Powers and Brownyard in 1948[36]. The model has since been modified and reanalysed, mainly by Powers, and is therefore called Powers' model.

A central feature of Powers' description is the division of evaporable water into gel-water and capillary water. Gel-water is a water phase that is adsorbed on the surface of solids. Capillary water is found in the larger voids and in the capillary pores beyond the range of the surface forces of the gel solid. As the capillary water is freely available for cement hydration it is also called free water.

The degree of binding of water can be given by the RH at which it is in equilibrium. In Powers' original model, described in PCA Bulletin 22[36], it is stated that gel-water is in equilibrium at RH from 0 to 100%. Capillary water is in equilibrium at RH 45-100%.

The relative amounts of the two types of water in the cement paste as a function of RH are shown by the sorption isotherm in Figure 3.

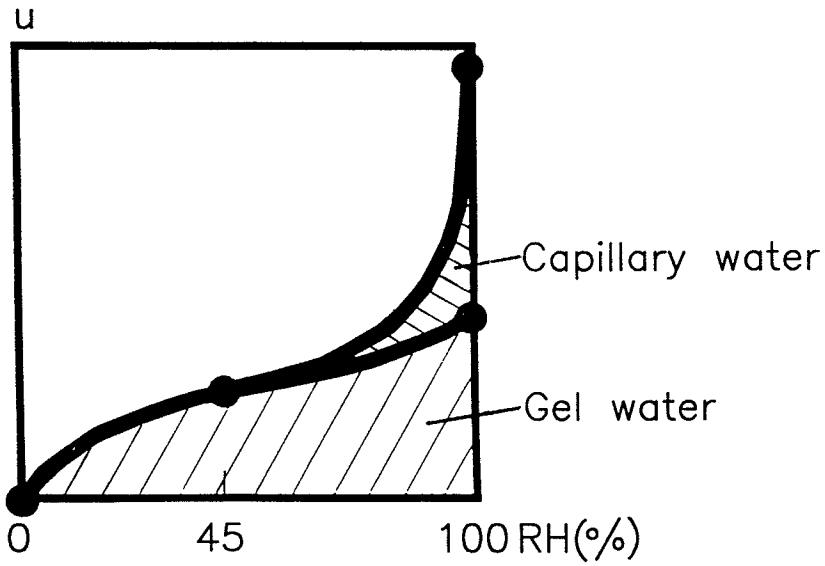

Figure 3. Schematic sorption isotherm for cement paste: Water content as a function of RH. In Powers' original model, gel-water is in equilibrium at RH = 0-100% and capillary water at RH = 45-100%.

In order to calculate self-desiccation Powers revised his model[56,22].

The argument is as follows, cf. Figure 3: RH-changes close to 100% will mainly affect the capillary water and only slightly affect the gel-water. Correspondingly, RH-changes in the interval 0 to approx. 80% will mainly affect the amount of gel-water.

The simplification of the original description is shown in Figure 4: Gel-water is in equilibrium at 0-100% RH and capillary water at 100% RH. This model is known as "Powers' simplified model".

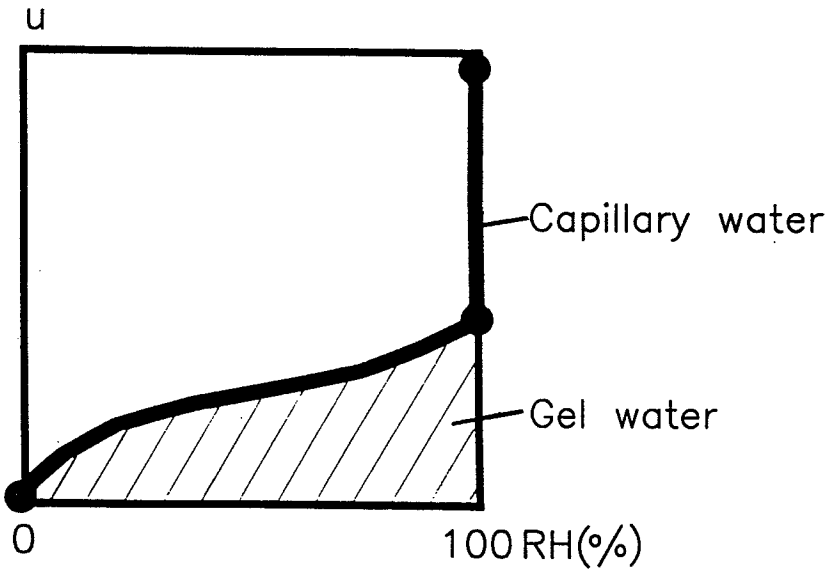

Figure 4. In Powers' simplified model gel-water is in equilibrium at RH = 0-100% and capillary water at RH = 100%. The capillary water is thus represented by the vertical part of the curve at 100% RH, and the gel-water by the amount of water below 100% RH.

The distinction between capillary water and gel water is abitrary, and the terminology may conflict with normal use of terms such as "capillary water" and "free water". Other interpretations of the concepts gel- and capillary water can be found in the literature[30], but they will not be discussed here.

The unique feature of Powers' model is that it quantifies the hydration process, and thereby makes it possible to calculate the self-desiccation.

According to Powers' simplified model, the capillary water is in equilibrium at 100% RH. A cement paste that hydrates in a closed system will therefore have an RH of 100% as long as capillary water is present.

When the capillary water has been used up, self-desiccation begins; the cement then begins to react with the more firmly bound gel-water, which is in equilibrium at RH <100% - the RH is lowered. There is a concomitant reduction in the speed of the reaction[56].

The following formulas describe the phase distribution in a hardening cement paste according to Powers' model:

$$V_{c.w} = \frac{w/c}{w/c + 0.32} - 1.4 \cdot \left(1 - \frac{w/c}{w/c + 0.32}\right) \cdot \alpha \qquad \text{(capillary water)} \qquad (1)$$

$$V_{g.w} = 0.6 \cdot \left(1 - \frac{w/c}{w/c + 0.32}\right) \cdot \alpha \qquad \text{(gel water)} \qquad (2)$$

$$V_{p} = 0.2 \cdot \left(1 - \frac{w/c}{w/c + 0.32}\right) \cdot \alpha \qquad \text{(gas-filled voids)} \qquad (3)$$

$$V_{ce} = \left(1 - \frac{w/c}{w/c + 0.32}\right) \cdot (1 - \alpha) \qquad \text{(cement)} \qquad (4)$$

$$V_{g.s} = 1.6 \cdot \left(1 - \frac{w/c}{w/c + 0.32}\right) \cdot \alpha \qquad \text{(gel solid)} \qquad (5)$$

For a given w/c, it is thus possible to calculate the volumetric relations as a function of the degree of hydration α.

When the w/c is lowered, there will be an increased consumption of capillary water. At a certain w/c, the capillary water will just suffice for complete hydration.

The w/c at which the cement will use all the capillary water for complete hydration is determined by $V_{c.w} = 0$ for $\alpha = 1$; the capillary water is used up at a degree of hydration of 1. If this condition is combined with (1), the w/c is found to be $\approx$0.45.

The resulting diagram can be divided into two cases: The volumetric relations are shown schematically in Figure 5 for w/c greater and less than 0.45 respectively. Note that the diagrams apply to a closed system - i.e. without transport of moisture to or from the surroundings. If evaporation takes place, the amount of capillary water will be further reduced.

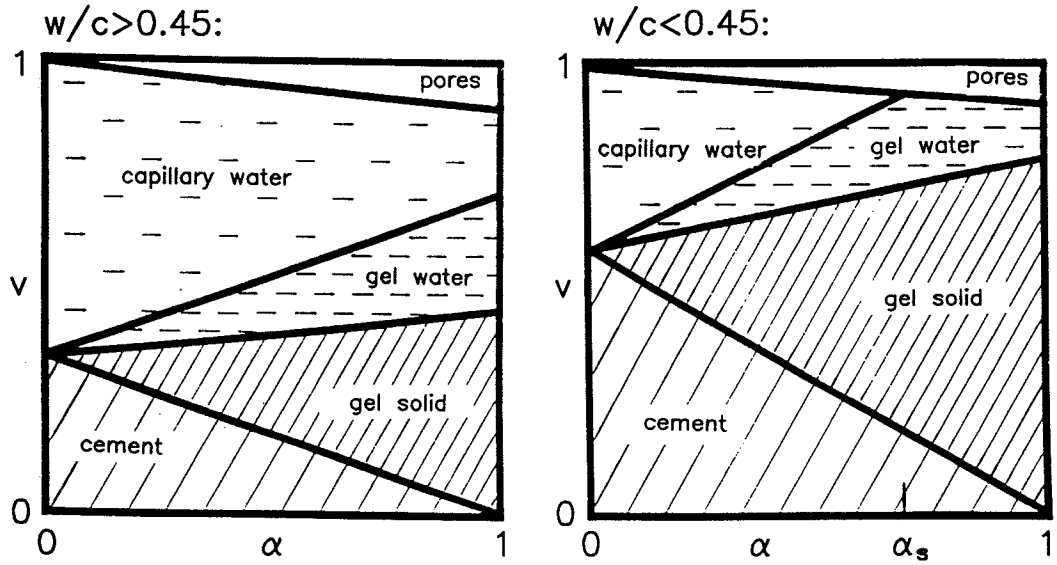

Figure 5. Volumetric amounts, V, for cement paste components as function of the degree of hydration α. At w/c <0.45 the capillary water is used up at a degree of hydration α_s.

In Figure 6 og Figure 7 the process is illustrated by sorption isotherms.

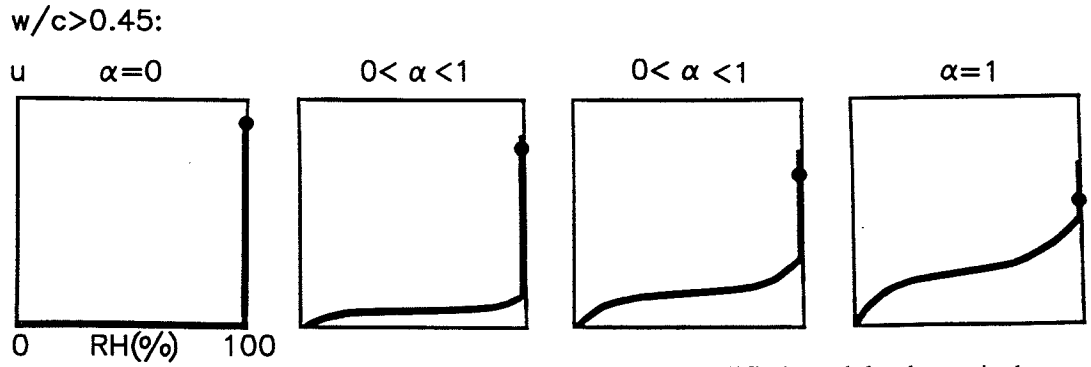

Figure 6. The hydration process according to Powers' simplified model schematically described by means of sorption isotherms. With a rising degree of hydration the capillary water is used, and the amount of gel-water increases. The point indicates the state after hydration in a closed system.

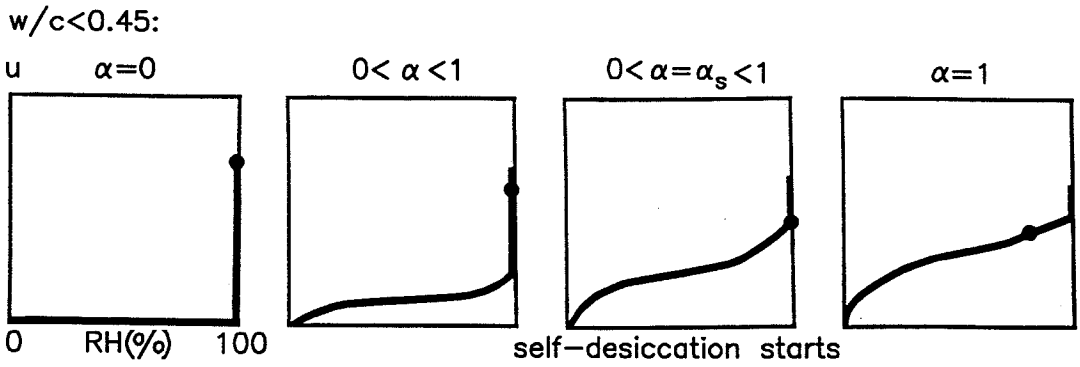

Figure 7. At w/c <0.45 all the capillary water is used during hydration. This results in the RH falling below 100%. Self-desiccation starts at $\alpha = \alpha_s$, cf. Figure 5.

If Powers' simplified model is taken to apply rigorously, self-desiccation will not take place in cement pastes with w/c >0.45. And for a cement paste with w/c <0.45, self-dessication will begin immediately at the degree of hydration at which the capillary water has just been used up.

Powers' simplified model should not be taken so rigorously; in reality the sorption isothermal is very steep close to 100% RH rather than vertical. A paste with w/c >0.45 may therefore have a slight lowering of RH from self-desiccation. Besides, at any w/c-ratio the relative humidity will be lowered due to dissolved salts in the pore fluid.

Neither the course nor the final level of self-desiccation can be calculated by Powers' model. At the present time only a qualitative description of the factors that determine the tendency of a cement paste to self-desiccate can be given:

1) The *pore structure* of the cement paste. A fine pore structure is potentially much more vulnerable to self-desiccation than a coarse structure. As an extreme example of a coarse pore structure, the relative humidity inside a bucket of water will stay at 100% even when all but the last drop of water is removed. On the other hand, if half the evaporable water of a well-hydrated cement paste is removed, the relative humidity may drop below 50%.

2) The *chemical shrinkage* accompanying the hydration. The chemical shrinkage is a measure of the amount of pore volume which has been emptied of liquid water due to cement hydration. Chemical shrinkage is therefore the direct cause of self-desiccation. Viewed separately, an increased chemical shrinkage will lead to an increased self-desiccation.

3) The *sensitivity to the relative humidity* of the hydration reactions (cement, silica fume and fly ash). A cement whose hydration is unaffected by a drop in the relative humidity will self-desiccate more vigorously than a cement which is sensitive to the relative humidity. If, for example, a cement is unable to hydrate below 80% relative humidity, self-desiccation will be restricted by this value.

When silica fume is added to cement paste a significantly stronger self-desiccation is observed[1]. This is not surprising because: 1) silica fume refines the pore structure of the cement paste[28], 2) the pozzolanic reaction of silica fume has a high chemical shrinkage compared to Portland cement[27], and 3) the pozzolanic reaction of the silica fume is relatively insensitive to a drop in the relative humidity[50].

3.2.2 RH-reducing mechanisms

Raoult's Law

Pure water is in equilibrium with air at 100% RH. A solution of salt in water is in equilibrium at RH <100%. To put it in everyday terms, the salt dilutes the water and thus lowers its activity.

The pore fluid in a cement paste contains dissolved salts. This results in a lowering of the RH. On the assumption of ideal solution and gas phase, the RH-lowering as a result of dissolved salts can be calculated from thermodynamic considerations[1]:

$$X_l = RH$$

This means that the relative humidity at equilibrium, RH, is equal to the molar fraction of water in the solution, X_l. This relation is known as Raoult's Law.

Raoult's Law is a good approximation when used for the pore fluid of cement paste with RH-lowerings of up to 5%[1] (e.g. 100% to 95% RH).

For cement paste it is mainly the salts of Potassium (K) and Sodium (Na) that give rise to a lowering of the relative humidity[57]. NaOH and KOH are highly soluble, in contrast to $Ca(OH)_2$ and $CaSO_4$, which contribute little to RH-lowering. If, for example, Raoult's Law is used on a saturated $Ca(OH)_2$ solution, it is found that:

$$RH \approx \frac{55.5}{55.5 + 3 \cdot 0.022} = 99.9\%$$

(The solubility of $Ca(OH)_2$ in water is 0.022 mol/l[48], and the molar volume of water is 55.5 mol/l at 20°C).

An example of values for ion concentrations in the pore fluid is given in Table 1. However, these values will depend on cement type, curing time, w/c, etc.

Na^+	K^+	Ca^{2+}	OH^-	SO_4^{2-}
263	613	1	788	23

Table I. Measured ion concentrations (mmol/l) in pressed-out cement paste pore fluid[67].

Kelvin's equation

RH-lowering in a pore system can also arise as a result of meniscus formation. A detailed description of this is given in Section 3.3.1. RH-lowering from meniscus formation can be calculated by means of the so-called Kelvin equation. Kelvin's equation, which can be derived thermodynamically[1], is given by (cf. Figure 11):

$$RH = \frac{p_g}{p_s} = \exp\left(-\frac{2\sigma M \cos\theta}{r\,\rho RT}\right)$$

Kelvin's equation applies to a pure water phase. If the water contains dissolved salts, the equation is modified. On the assumption that Raoult's Law applies, the following expression can be derived[1]:

$$RF = \frac{p_g}{p_s} = X_l \cdot \exp\left(-\frac{2\sigma M \cos\theta}{r\,\rho RT}\right)$$

This formula is extremely simple; the RH resulting from simultaneous meniscus formation and dissolved salts is the product of the RH value from meniscus and that from salts.

θ is the angle of contact between the fluid and the solid. It is a function of the relative humidity[47] and of dissolved salts[45] in the pore fluid. As θ is difficult to determine, it is normally taken as 0°, corresponding to $\cos(\theta) = 1$[47,54].

The value 0° is not completely arbitrary. For silicates such as quartz and orthoclase the contact angle is in fact[43] 0°, and for all materials it is theoretically[41] 0° at 100% RH. Furthermore, $\cos(\theta)$ is insensitive to changes in θ near 0°; e.g. $\cos 20° = 0.94 \approx 1$.

σ is the surface tension of the fluid. The value for pure water - approx. 73 mN/m - is often used. This value, however, is unrealistic in practice. It applies only to extremely pure water, e.g. triple-distilled. Measurements show that a value of approx. 55 mN/m is more realistic[1].

3.3 Autogenous deformation

Autogenous deformation arises as a result of internal processes; it is the unhindered deformation of a hermetically sealed specimen at constant temperature. Many deformation mechanisms may be active under these conditions.

With regard to self-desiccation and self-desiccation shrinkage, the mechanisms associated with RH-changes are of special interest, cf. Section 3.1. These mechanisms have been investigated by many notable cement researchers, but many problems still remain unsolved. There is much disagreement on which mechanisms are dominant in a given RH-interval, cf. Figure 8.

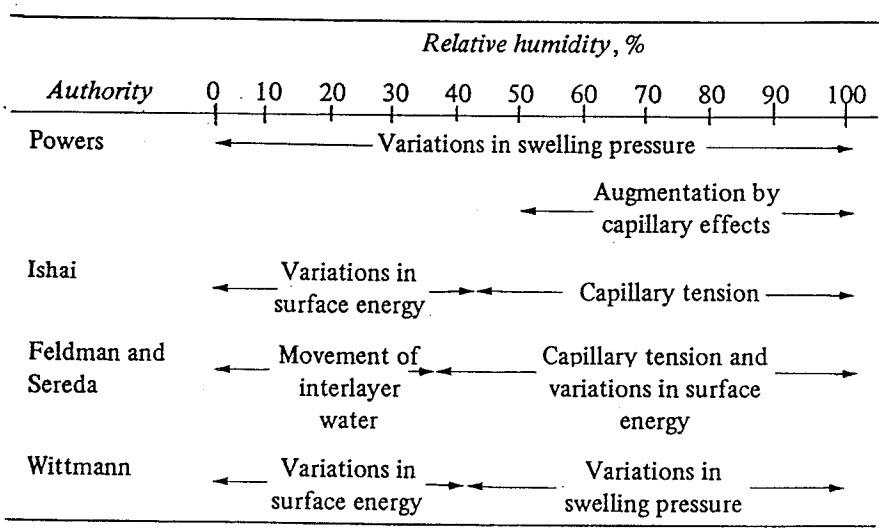

Figure 8. Applicability intervals for deformation mechanisms according to various researchers[39]. In the high RH-interval, 70-100%, in which self-desiccation occurs, capillary tension is frequently given as the dominant cause of deformations.

Even if the active deformation mechanism(s) were known, the deformations would be difficult to calculate. Only for a few mechanisms is it possible to set up simple numerical expressions for the stresses that arise, and the relation between local microstress and bulk deformation is far from clear.

The functioning areas must be taken into account in evaluating the mechanisms. The capillary stresses are e.g. active in the fluid phase, while the crystallization pressure arises only in the limited contact areas in which crystal growth is hindered.

It is also important to take the deformation properties of the solid "skeleton" into account. These manifest themselves via the modulus of elasticity. A given stress loading results in greater deformations when the modulus of elasticity is low, e.g. at a low degree of hydration. Attention must also be given to creep.

The mechanisms discussed in Sections 3.3.1-3.3.4 are associated with the paste. In a concrete or mortar, deformations can also arise as a result of reactions with the aggregate, e.g. expansive alkali-silica reactions between alkalis in the cement and silica in the aggregate. In addition, the rigid aggregate will have a mechanical damping effect on the deformations, cf. Figure 9.

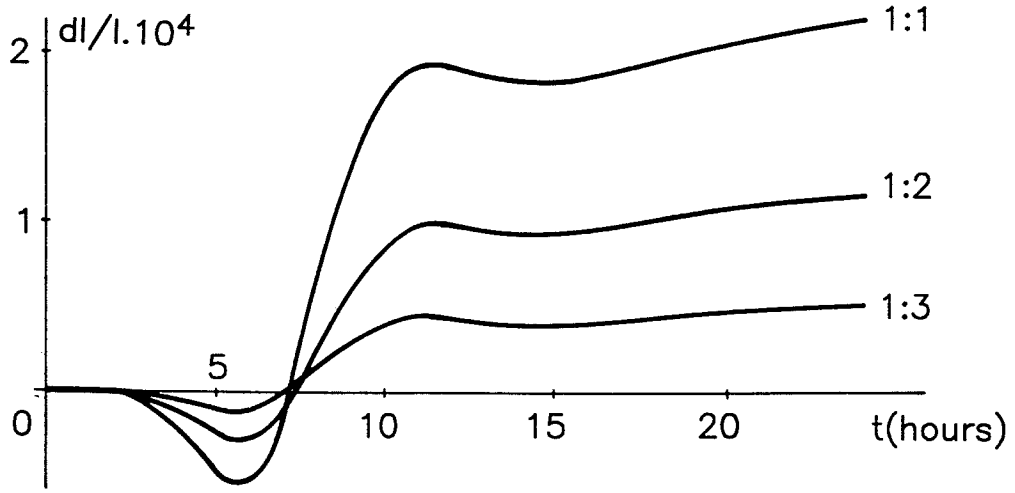

Figure 9. Influence of the aggregate on deformations in mortar and concrete[55]. The effect shown is due to the stone and sand particles acting as restainers. An increased amount of aggregate damps drying shrinkage. The tests were carried out on mortars with cement/aggregate ratios as shown. The curve shows autogenous deformation with superimposed drying shrinkage, as the specimens were cured at approx. 60% RH.

Modelling the autogenous deformation of concrete is further complicated by the large number of parameters involved: w/c, silica fume content, additives, cement type (which again has many parameters), etc. Another important parameter in relation to concrete is the water absorption capacity of the aggregate. The water in the aggregate particles subdues the self-desiccation of the cement paste and thereby reduces the resulting self-desiccation shrinkage.

Because of the many influencing parameters, autogenous deformation is most often treated phenomenologically in the literature. There are few examples of physical, chemical or thermodynamic analysis of the underlying mechanisms that make a prediction possible.

A description of the action of micromechanisms on autogenous deformation has not yet found its final form. This does not prevent the analysis and modelling of autogenous deformation at the experimental level. Measurements given in the literature indicate that:

□ Autogenous deformation and temperature deformation can be simply superimposed[17].

□ Autogenous deformation is a thermally activated process[17,46]. The influence of temperature on the development of autogenous deformation can apparently be described by e.g. an Arrhenius expression in the same way as for cement hydration. This is in contrast to theoretical considerations which show that the maturity concept is not applicable to autogenous deformation[12].

□ The addition of silica fume can result in a considerable increase in autogenous deformation and autogenous RH-change[15,13].

An example of a model that apparently predicts the autogenous deformation of concrete is given by Larrard and Roy[40].

3.3.1 Capillary tension

A plane water surface is in dynamic equilibrium with saturated water vapour, RH = 100%. In a given time, as many molecules will evaporate as return from the gaseous phase.

A concave liquid surface will be in equilibrium at a lower vapour pressure, RH <100%. As shown in Figure 10, this can be popularly explained by saying that the curvature reduces the escaping tendency of the liquid particles.

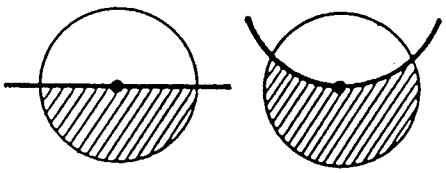

Figure 10. A water molecule in a concave liquid surface is held by a greater number of adjacent molecules than in a plane surface. Attractive forces from neighbouring molecules act within the hatched area[39].

The relation between the radius of curvature of the liquid surface and the RH can be derived thermodynamically[1]. The result is given by Kelvin's equation:

$$RH = \exp\left(-\frac{2\sigma M \cos\theta}{r\rho RT}\right)$$

The relation is shown graphically in Figure 11.

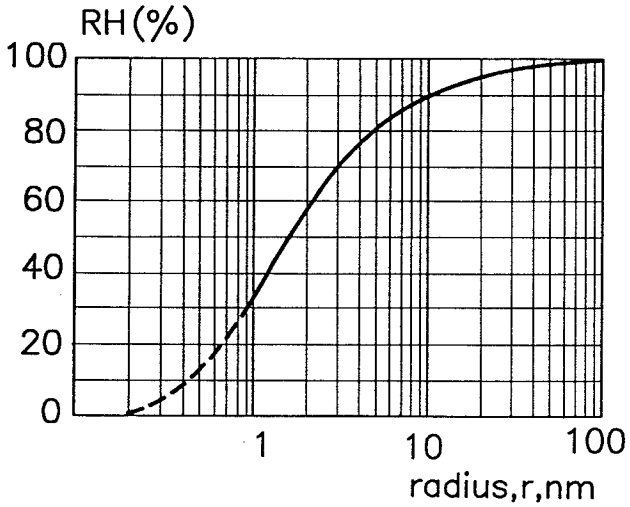

Figure 11. RH as a function of the radius of curvature of the meniscus for water at 20°C[32]. The curve is stippled for r <1 nm, as it is meaningless to talk of a radius of curvature for a meniscus composed of a few molecules. A semicircular meniscus with r = 1 nm will consist of 10 water molecules, the length of each molecule being approx. 0.3 nm.

The RH-lowering and the meniscus curvature are associated with a change of pressure in the liquid phase. The following expression can be derived[1]:

$$p_l = \frac{\rho RT}{M} \cdot \ln RH \qquad (6)$$

The fluid stress, p_l, can be seen to be negative for RH <100%, corresponding to a tensile stress. The expression does not take atmospheric pressure into account. The relation is shown in Figure 12.

The Figure shows that the tensile stress in the fluid phase is considerable even with a modest RH-lowering. This must be balanced by a compressive stress in the surrounding solid material. The deformation will depend on the modulus of elasticity and the geometry of the solid.

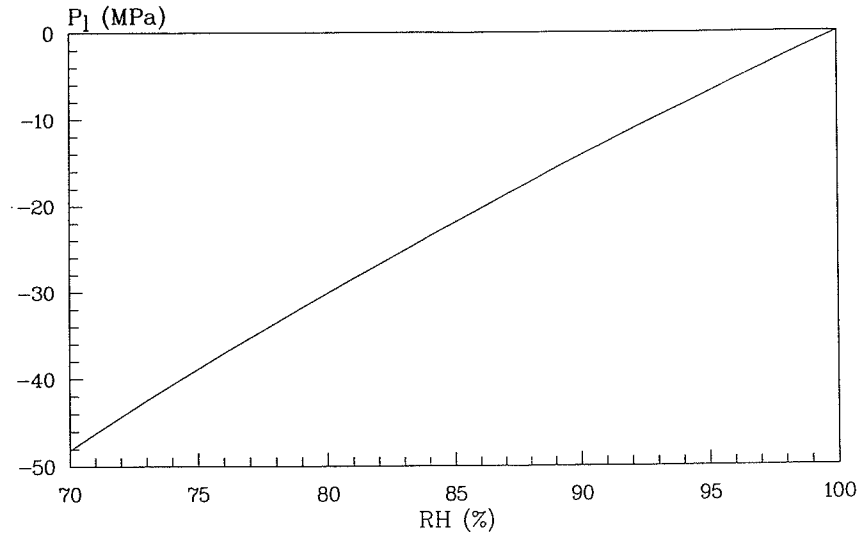

Figure 12. Stress in the fluid phase as a function of RH for pure water at 20°C according to Kelvin's equation. Atmospheric pressure is not included.

3.3.2 Disjoining pressure

As a result of van der Waals' forces, water molecules can adhere to the surface of a solid. The water molecules form a compact, orderly structure - they are said to adsorb to the surface. See Figure 13.

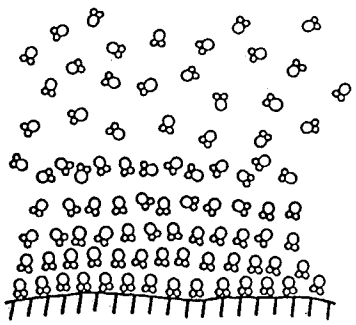

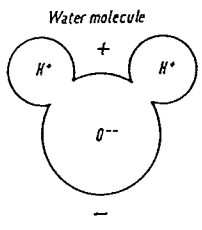

Figure 13. Schematic picture of adsorption. Water molecules are acted upon by surface forces from a solid. This results in an orientation and compaction of the water. Based on Winkler[35].

At equilibrium the thickness of the adsorbed water layer is a function of RH. The relation is shown in Table II.

Relative humidity (%)	Thickness	
	Å	molecular diameters*
5	2·00	0·76
10	2·45	0·95
15	2·80	1·06
20	3·05	1·16
30	3·40	1·30
40	4·25	1·62
50	5·15	1·96
100	13·00	5·00

* Diameter of adsorbed water molecule = 2·63 Å.

Table II. Corresponding values of RH and the thickness of the adsorbed layer of water molecules (t-layer). From Powers[37].

Figure 14 shows a situation in which two particles are so near each other that there is no room for a fully adsorbed layer at the surfaces. The water between the particles will then try to press them away from each other - the so-called disjoining pressure. The less space available for the adsorbed water, relative to the thickness corresponding to the RH, the higher the pressure that can be built up.

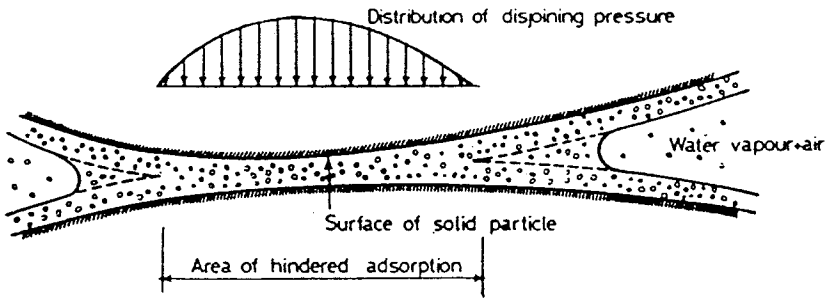

Figure 14. In the areas where there is insufficient space for the adsorbed layer to build up to the thickness corresponding to the RH of the ambient air, disjoining pressure arises. Based on Soroka[39].

When RH is falling, the thickness of the adsorbed layer is reduced, thereby reducing the disjoining pressure. The relation between RH in the vapour phase and pressure change in the fluid phase due to disjoining pressure can be derived thermodynamically[1]. The result is:

$$\Delta p = \frac{\rho RT}{M} \ln RH$$

Note the similarity to the formula for capillary tension, (6).

3.3.3 Surface tension

Both fluids and solids have a surface tension. A molecule in the interior of a solid is held by the surrounding molecules on all sides. On the other hand, a molecule at the surface is attracted only from the interior and tangentially at the surface. As a result, the surface behaves as a stretched elastic membrane. The surface tension can be regarded as the stress in this fictitious membrane.

For example, when water is adsorbed on the surface of a solid, the surface tension is changed. This is because the surface molecule in the solid is now subjected to outward molecular forces, thus reducing the surface tension. See Figure 15.

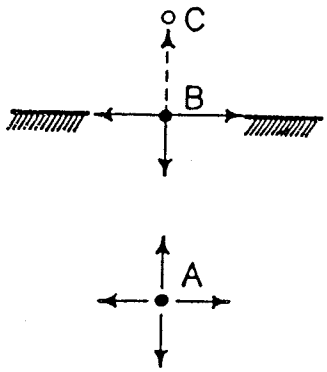

Figure 15. By the adsorption of a water molecule C, the surface molecule in the solid B approaches the state of a molecule in the interior of the solid A[39].

The surface tension in a particle gives rise to an inner compressive stress. Adsorption changes the surface tension and thereby changes the compression. According to Powers[37] the change in compression is given by:

$$\Delta p = \frac{2}{3} S \Delta\sigma (RH)$$

where S is the specific surface of the particle and $\Delta\sigma$ the change in surface tension. The change in the surface tension of the solid depends on the amount of adsorbed water and thus on RH.

The expression shows that the pressure change is proportional to the specific surface. If all other factors are constant, this mechanism will therefore have a greater effect on a material with a large inner surface than on one with a small inner surface as, for example, brick.

3.3.4 Other mechanisms

Chemical shrinkage

Consider situation A in Figure 16, where a small air bubble is in a cylinder of water enclosed by a piston. The system is in pressure equilibrium with the surroundings, i.e. the pressure in the water, the bubble and the surroundings is 1 atmosphere. (The bubble is large enough to make capillary forces negligible).

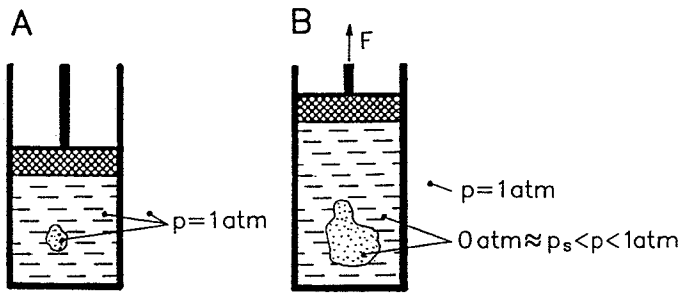

Figure 16. In a volume of water containing air bubbles the pressure cannot sink below approx. 0 atm. This corresponds to a pressure drop of 1 atm. An explanation is given in the text.

In situation B the piston is subjected to an outward force that results in an expansion and a fall in pressure in the water. As water is incompressible in comparison with air, the air bubble will expand when the piston rises. The lowest pressure that can exist in an air volume is 0 atm, a vacuum. As the air is surrounded by water, evaporation will take place until the air is saturated with water vapour. The pressure therefore cannot fall below that of saturated water vapour, p_s, which at 25°C is 3167 Pa = 0.03 atm ≈ 0 atm[49].

The lowest water pressure is thus approx. 0 atm. This corresponds to a pressure of 1 atm. on the piston.

The system shown in Figure 16 is analogous to a hardening cement paste. As the hydration products take up less space than the reacting water and cement, the pore fluid will be affected in the same way as in Figure 16, B; in a hardened cement paste the outer volume is practically constant. The piston movement corresponds to the chemical shrinkage. The result is air-filled pores in the cement paste.

The lowest hydrostatic stress in the pore fluid of a cement paste, in the absence of capillary forces, is therefore approx. 0 atm. The reduction in the fluid stress increases the compressive stress in the solid "skeleton". The magnitude of the compressive stress in the "skeleton" depends on geometrical factors; if the "skeleton" comprises a small part of the cross-section of the paste the stresses will be high, and vice versa.

In the very early hydration phase the solid skeleton is weak. If it cannot bear the "suction" from the water, it will collapse. Chemical shrinkage will then appear as an outer shrinkage - pore formation will not take place until the skeleton is sufficiently strong. This mechanism is mentioned by Setter and Roy[9], Geiker[31] and others.

The above description applies as long as there are relatively large water-containing pores in the cement paste. When these have been emptied, high tensile stresses will arise in the pore fluid; the water is sucked into the narrow capillary pores. According to Powers' simplified model this will occur only in pastes with w/c <0.45, cf. Figure 5.

Crystallization pressure

The crystallizing out of salts can build up pressure if the growth of the crystals is hindered[35].

The theoretical maximum contact pressure that a crystal can build up can be derived thermodynamically[34]:

$$p_{cryst} = \frac{RT}{V_S} \ln \frac{C}{C_S}$$

where p_{cryst} is the contact pressure during crystal growth, C the actual salt concentration and C_s the salt concentration at saturation.

Oversaturation of the pore fluid is necessary to build up the crystallization pressure. As the formula shows, the crystallization pressure depends on the degree of oversaturation in the pore fluid C/C_s. For many salts it has been found experimentally[35] that the degree of oversaturation cannot exceed approx. 100.

In the literature, ettringite crystallization is frequently given as a cause of expansion[42]. Using the tabulated data for ettringite, the maximum contact pressure is found to be:

$$p_{cryst} = \frac{8.314 \cdot 298.15}{(1237.22/1.73) \cdot 10^{-6}} \ln 100 = 16\ MPa$$

as $V_s = M_s/\rho_s$.

Hydration pressure

The taking up of water by the solid material in the process of hydration increases the volume of the solid component. This can result in the build-up of pressure.

The process $CaSO_4 \cdot \frac{1}{2}H_2O + 1\frac{1}{2}H_2O \rightarrow CaSO_4 \cdot 2H_2O$ which takes place during false setting of Portland cement, can result in a pressure of up to 150 MPa[35].

The following expression for calculating the maximum hydration pressure is given by Winkler[33]:

$$p_{hydr} = \frac{nRT}{V_h - V_a} \ln \frac{p_w}{p_w'}$$

where n is the number of moles of water taken up in hydration, V_h and V_a the molar volumes of salt after and before hydration respectively, p_w the water vapour pressure with which the reacting water is in equilibrium, and p_w' the equilibrium water vapour pressure for the hydrated salt.

The hydration of CaO and MgO can cause harmful expansions in hardening concrete. While the $CaSO_4 \cdot \frac{1}{2}H_2O$ hydration proceeds so rapidly that it takes place only in the plastic phase, the MgO reaction is very slow. Damage frequently appears only after several years[29].

The hydration pressure is an expansion mechanism, but the reverse process can result in shrinkage. RH-lowering can result in the hydrates becoming thermodynamically unstable and dehydrating. The associated volumetric reduction can cause an overall shrinkage.

Water in certain aluminate hydrates is relatively loosely bound; they dehydrate at moderate temperatures[29]. Dehydration can also take place as a result of low RH.

Osmotic pressure

When a solution of salt in water is brought into contact with pure water through a semipermeable membrane, the water will pass through the membrane to equalize the difference in concentration. The phenomenon is called osmosis and can result in a build-up of pressure if the transport of water is hindered - an osmotic pressure. See Figure 17.

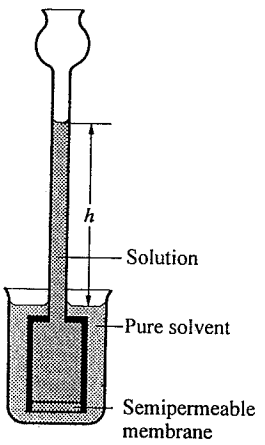

Figure 17. Osmosis illustrated by pressure build-up. The salt solution and the pure water are separated by a membrane that only permits the passage of water molecules. The difference in salt concentration produces an osmotic pressure, which, in equilibrium, can be measured as the height of the liquid column, h. Based on Atkins[24].

For dilute solutions the following formula for calculating the osmotic pressure p_{osm} can be derived thermodynamically[24]:

$$p_{osm} = R \cdot T \cdot C$$

where C is the molar concentration of the dissolved species. A salt concentration of e.g. only 1 mole KOH/l will produce an osmotic pressure on pure water of approx. 5 MPa. Salt concentrations of this order exist in the pore fluid of cement paste, cf. Table I.

According to Powers' description[36], the pores of the cement gel are so narrow that the water they contain - the gel-water - is bound by adsorption, cf. Figure 13. The salt ions may not be able to penetrate into this compact water phase[35]. Osmotic effects between the gel-water and the capillary water can therefore be expected. If the salt concentration in the capillary water increases, tensile stresses in the gel-water will arise due to osmosis. This will cause shrinkage in the cement paste.

A difference in salt concentration can also arise if the gel pores have narrow passages. The salt ions are hydrated, i.e. bound to the surrounding water molecules, and are thereby considerably larger than water molecules. Pores can thus be permeable for water but impermeable for salt ions.

Electrical surface forces

Particles of colloidal size (less than about 1 μm) in a salt solution are normally electrically charged. This is probably due to the adsorption of salt ions on the surface of the particles. The electrical charges are important for the stability of colloid particle systems. A change in the salt concentration of the solution can cause a neutralization of the charges on the colloid particles, resulting in their coagulation.

The products of cement hydration are of colloidal size. It is therefore possible that electrical forces cause deformations in the cement paste. The electrical charges carried by the gel particles will change when the salt concentrations in the pore fluid of the cement paste change. The electrical forces of attraction and repulsion between the gel particles will hereby also be modified. Salt concentrations in the pore fluid change considerably during hydration, and the solubility of salts depends - inter alia - on the fluid stress and thus on RH, cf. Kelvin's equation.

This deformation mechanism is not often mentioned in cement literature - a detailed account is given by Buil[26].

Restrainers

$Ca(OH)_2$ crystals are considered by some researchers as shrinkage restrainers[9]. The crystals are assumed to carry the solid skeleton and thereby hinder shrinkage in the same way as aggregate in concrete. See Figure 9. This hypothesis is also advanced by Powers to explain carbonation shrinkage in concrete[25]. According to Powers, the $Ca(OH)_2$ crystals under pressure dissolve during the carbonation process and thereby release the restrained shrinkage.

The mechanism is also interesting in connection with an explanation of autogenous deformation from pozzolan additives. Silica fume uses $Ca(OH)_2$ in the pozzolan reaction. This will result in shrinkage if the $Ca(OH)_2$ crystals are under pressure.

Other components can also be assumed to act as restrainers, e.g. the silica fume particles. The mechanism is sketched in Figure 18.

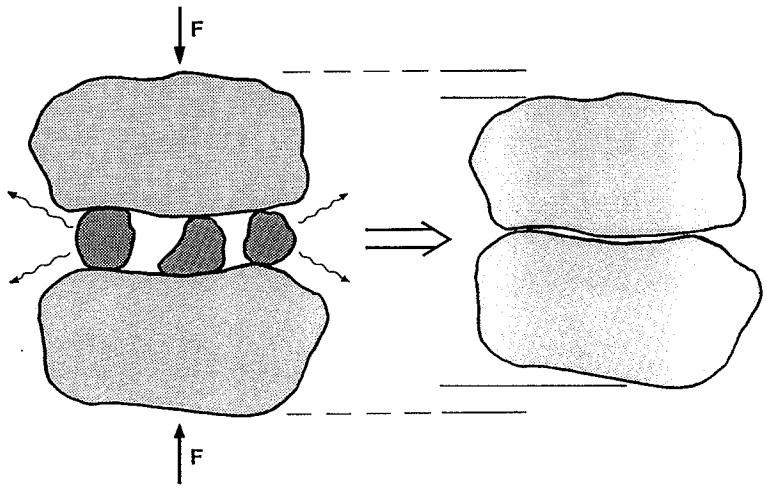

Figure 18. Simplified illustration of restrainer shrinkage. Particles dissolving under pressure induce shrinkage.

It is important to note that the mechanism is unconnected with RH-changes, i.e. it can cause shrinkage at a constant RH.

Interlayer water

According to the theories of Ishai and others, the layered structure of the cement gel contains pockets of enclosed water - "interlayer water"[39]. During the drying process, this water will move out, causing a collapse of the solid structure and thereby inducing shrinkage. According to Ishai, complete re-wetting is not possible and the mechanism thus results in an irreversible shrinkage.

4 Measuring techniques in the literature

4.1 Autogenous RH-change

The relative humidity of the air can be measured in many ways. Moisture-sensors for continuous measurements in the laboratory generally use one of the following three principles: capacitive measurement, impedance measurement or dew-point measurement. None of them are very accurate - after careful calibration the uncertainty can be brought down to ±1% RH.

When measuring the autogenous RH-change of cement paste, loss of moisture from the test specimen can contribute much more to the uncertainty than the sensor's lack of precision. The RH is particularly affected by moisture loss in pastes with silica fume and low w/c. It is precisely these pastes that are interesting with regard to self-desiccation.

Repeated measurements on the same specimen, in which the sealing is broken at each measurement[51,53,61], or in which the specimens are stored in plastic bags[64,68], plastic containers[71] etc. can involve moisture losses that greatly affect the result.

Measurements are normally carried out on crushed paste, which rapidly arrives at a moisture equilibrium with the sensor. See Figure 19. In some cases, however, the sensor is placed in a cavity in the test specimen[38,58,59,69].

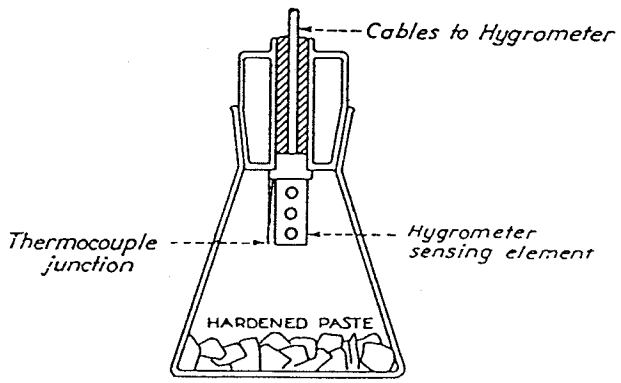

Figure 19. Frequently used set-up for the measurement of autogenous RH-change[22]. Crushed cement paste is placed in a small enclosed volume with a moisture sensor.

4.2 Autogenous deformation

Measurement of autogenous deformation has been carried out in two fundamentally different ways: measurement of volumetric deformation and measurement of linear deformation.

Volumetric measurement of autogenous deformation is frequently performed by placing the fresh cement paste in a tight rubber balloon immersed in water. The change in volume of the cement paste is measured by the amount of water displaced by the immersed sample, for example, by measuring the change in weight of the immersed sample (buoyancy). Volumetric measurement of autogenous deformation has been performed by a number of researchers[2,4,5,9,14,63,66,70,73].

Linear measurement of autogenous deformation is frequently performed by placing the cement paste in a rigid tube with low friction. The change in length of the cement paste is recorded by a displacement transducer at the end of the specimen. Linear measurement of autogenous deformation has been performed by a number of researchers[3,20,21,26,44,46,60,62,65,72].

Both methods of measurement have advantages and disadvantages. One advantage of the volumetric method is the possibility of commencing the measurements immediately after casting. In contrast, the lack of a steady contact between the rubber balloon and the cement paste is a considerable disadvantage of the volumetric method. Bleeding water or entrapped air at the surface of the cement paste may obstruct this contact significantly. During the hydration process the bleeding water or entrapped air will be sucked back into the cement paste as a consequence of internal volume reduction caused by chemical reaction. Since the volume of the rubber balloon is the combined volume of the cement paste and the volume of the bleeding water of entrapped air, the internal volume reduction also may be measured erroneously as an outer deformation. Since the internal volume reductioin is considerably larger than the autogenous deformation this may lead to a substantial error.

In addition, Buil[26] mentions that the pressure caused by a tight rubber balloon could damage the weak structure during setting. Furthermore, volumetric measurements of autogenous deformation are normally associated with large scatter of the data. Based on experimental data Buil[26] and Baron and Buil[20] conclude that the volumetric method seems less suitable for measuring autogenous deformation.

One advantage of the linear method is the firm anchorage of the measuring point to the cement paste. This reduces the above-mentioned problems greatly. At the same time this is a disadvantage since the measurements cannot be started before the cement paste has set. The linear method has an additional problem: the risk of restraining the cement paste. In the very first hours after setting, the cement paste is too weak to overcome the friction against a rigid tube, However, this problem can be reduced by lubricating the tube.

5 Tests

5.1 Measuring equipment

5.1.1 Paste dilatometer

For measuring the autogenous deformation of mortar, the dilatometer and form system shown in Figure 20 was used. The equipment was developed for the measurement of paste[11], but was used in the present project for mortars with a maximum particle size of 1 mm.

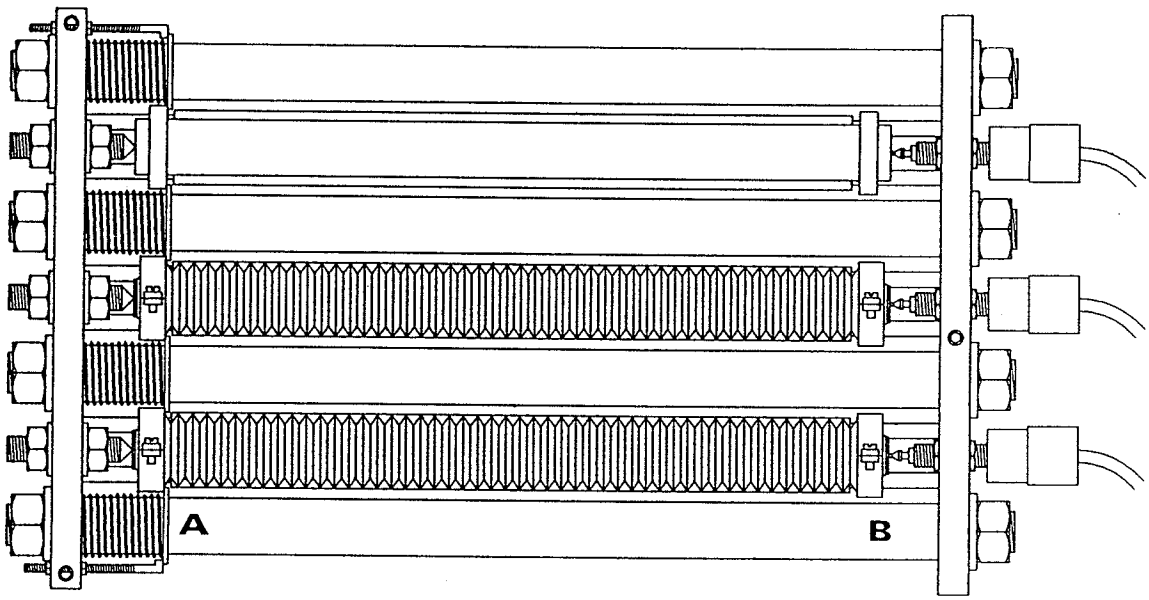

Figure 20. Dilatometer with two test specimens and one reference rod (uppermost). The specimens are fixed at A with spiral springs, and the changes in length are registered by displacement transducers at B. The length of the samples is approximately 280 mm.

The equipment measures the linear deformation of the specimen, cf. Section 4.2. The special feature of the equipment is that measurements can begin before setting. A special form system of corrugated tubes, shown in Figure 20 enables this to be done. The corrugation permits the tubes to deform easily in the longitudinal direction, and the geometry of the cross-section is well-defined. The sealing prevents exchange of material with the surroundings (CO_2 and H_2O).

While measuring is in progress the equipment is immersed in a thermostatic bath, the temperature of which is regulated with an accuracy of ±0.1° C. The close contact with the thermostat fluid ensures effective temperature control of dilatometer and test specimens.

Simultaneous measurements were made on two test specimens and a reference rod of invar. The measurement on the reference rod was used to check the operation of the electronic instruments. During the tests the signal from the reference rod varied by approx. 1 μm (approx. 3 μstrain).

The two test specimens are always of the same mortar.

Mixing, casting and mounting in the dilatometer takes about 20 minutes. The measurements began 30 minutes after the addition of water.

Transducer signals and temperatures at chosen points were registered automatically at 15-minute intervals and transferred to a coupled datalogger.

5.1.2 Concrete dilatometer

Autogenous deformation of concrete is measured with a concrete dilatometer, see Figure 21. The concrete dilatometer and its form system function in principle in the same way as the paste dilatometer described in the previous Section.

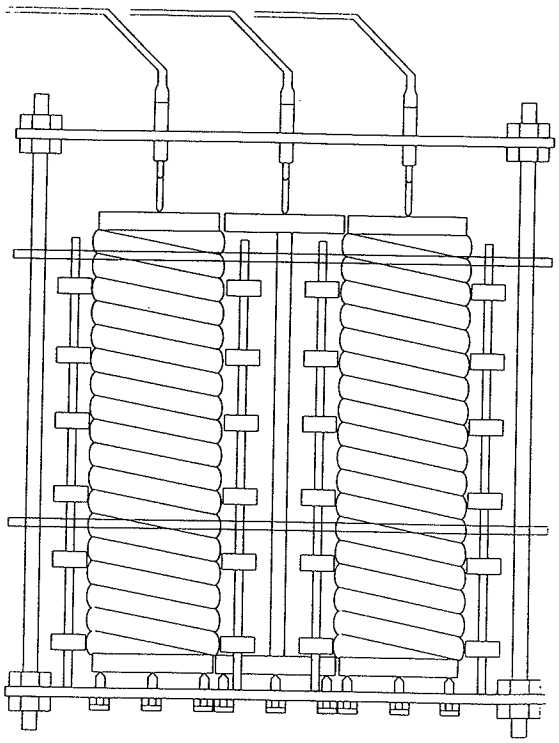

Figure 21. Sketch of dilatometer for the measurement of autogenous deformation of concrete. Two test specimens and an invar reference rod are measured simultaneously. The specimens are vertical, and are supported by sliding plates of teflon. Changes in length are measured by displacement transducers placed above. The forms are Ø100 · 375 mm long flexible tubes.

The forms are closed by metal plates that act as contact surfaces for the transducers.

During measurement the equipment is immersed in a water bath in which the temperature is regulated with an accuracy of ±0.1°C.

Mixing, casting and mounting in the dilatometer lasts approx. 50 minutes. The first measurement is carried out after one hour. The measurements are transferred to a datalogger at 15-minute intervals; they include changes in length and the temperature at the centre of each test specimen.

The dilatometer frame is of steel. The deformation of the dilatometer due to temperature changes must therefore be taken into account. The dilatometer deformation is determined by measurements on invar reference rods. The correction, which amounts to approx. 15 μstrain/°C, is made by means of measurements described in the following Sections. The correction is significant only when measurements are carried out during controlled temperature cycles.

5.1.3 Moisture measuring equipment

Autogenous RH-change in hardening mortar is registered by a moisture measuring equipment of the type Rotronic Hygroscope DT. The measuring station contains a temperature sensor and an RH sensor.

The measuring stations are placed in a climate-chamber in which the temperature is controlled with an accuracy of ±0.1°C.

Before and after each test the RH sensors are calibrated with saturated salt solutions of K_2SO_4 (≈97% RH), KNO_3 (≈92% RH), KCl (≈84% RH) and NaCl (≈75% RH). The uncertainty in measurement in the 75-100% RH interval is thereby reduced to ±1% RH.

Moisture loss from leakage in the chambers and inadequate calibration can result in large errors in measurement[10]. To reveal such errors, measurements are made at four stations simultaneously.

Some of the measurements are made on crushed mortar. This means that the mortar must be hardened. During the hardening the mortar is placed in moisture-tight teflon casting forms in a climate-chamber. To counteract bleeding the forms are continuously rotated during hardening. After removal of the forms the mortar is crushed. About 10 g of the crushed mortar is immediately placed in the moisture measuring stations.

Signals from the RH sensors and thermoelements are registered automatically at 15-minute intervals and the data stored in a coupled datalogger.

5.2 Sample preparation

Two concrete mixes and the corresponding mortars were investigated in this project: 1) A typical structural concrete used by the Danish Road Directorate, and 2) An alternative mix. In the following these concretes are referred to as "Road Directorate concrete" and "alternative concrete".

The composition of the mortars is the same as that of the corresponding concretes, except that aggregate larger than 1 mm was removed by sieving prior to mixing.

Originally it was planned to carry out measurements on the cement paste of the Road Directorate concrete. The initial measurements showed, however, that the early phase of hardening deviated markedly from that of the concrete. The setting time of the paste was approx. 14 hours at 40°C, that of the concrete 5 hours at 20°C. An investigation showed that this was due to an interaction between the superplasticizer and the finest aggregate fraction. For this reason the originally planned experiments on cement paste were replaced by measurements on mortar, described below.

5.2.1 Materials

Road Directorate concrete

The composition of Road Directorate concrete is shown in Table III.

Component	kg/m^3
Cement, low-alkali, sulfate-resistant	285
Fly ash	60
Silica fume	12
Water	127
Sand 0-4 mm, RN Avedøre	758
Aggregate 8/16 mm, SC Rønne	535
Aggregate 16/25 mm, SC Rønne	565
Air-entraining agent, Conplast 316 AEA	0.357
Plasticizer, Conplast 212	1.428
Superplasticizer, Peramin FF	2.856

Table III. Composition of Road Directorate concrete (kg/m^3). The silica fume is added as slurry, containing 50% water. The stated amount of silica fume is the dry weight, and the stated amount of water includes that in the slurry. The weights of sand and aggregate correspond to a water-saturated, surface-dry state. The water absorption is 0.2% for both aggregate fractions and 0.4% for the sand. The uncorrected w/c ratio is 0.45. The equivalent w/c ratio is 0.38. Water in the additives is included in the w/c.

The sand in the Road Directorate mortar comprises the fraction passing a 1 mm sieve. This amounts to 531 kg/m^3 (70% of the total sand).

Alternative concrete

The composition of the alternative concrete is shown in Table IV.

Component	kg/m^3
Cement, basis cement	320
Fly ash, Danaske	58
Silica fume, powder	20
Water	156
Sand 0-4 mm, RN-Avedøre	550
Aggregate 8/16 mm, Dalby	705
Aggregate 16/24 mm, Dalby	488
Air-entraining agent, SikaAer-15B	1.91
Plasticizer, Sika Plastiment-A40	2.82

Table IV. Composition of alternative concrete (kg/m^3). The weights of sand and aggregate correspond to a water-saturated, surface-dry state. The uncorrected w/c ratio is 0.49. The equivalent w/c ratio is 0.41. Water in the additives is included in the w/c.

The sand in the alternative mortar comprises the fraction passing a 1 mm sieve. This amounts to 373 kg/m^3 (68% of the total sand).

5.2.2 Mixing

Mixing procedure

The mortars are mixed for five minutes in a 5-litre mortar mixer. About 1½ litres of mortar are mixed for deformation and RH measurements. Immediately after mixing two form tubes are filled with mortar for deformation measurements and four Ø14·100 mm teflon forms for RH tests. Casting is carried out on a vibration table.

The concretes are mixed for four minutes in an 80-litre pan-type mixer. About 20 litres are mixed. The slump, air content and density of the fresh concrete are measured, and two flexible tubes are filled with concrete on a vibration table for deformation measurements.

The materials used are stored and cast at room temperature, approx. 20°C. The sand and aggregate are in a water-saturated, surface-dry state prior to mixing.

5.2.3 Summary of experiments

A summary of the experiments carried out is given in Table V.

	Approximate thermal history	Autogenous deformation		Autogenous RH-change, (mortar)
		Concrete	Mortar	
Road Directorate concrete	20°C	2	2	4
	40°C	2	2	4
	20-40-20°C	2	2	-
Alternative concrete	24°C	2	2	4
	40°C	2	2	-
	24-40-24°C	2	-	-

Table V. Summary of experiments carried out. The figures show the number of samples for each experiment. The exact thermal history is described by the respective graphs for the experiments.

5.3 Results

The following figures show measurements of autogenous deformation and autogenous RH-change of mortar and concrete. The measurements have been performed at two temperature levels: approximately 24°C and 40°C. Time is given in real hours from water addition. Shrinkage is plotted as negative deformation.

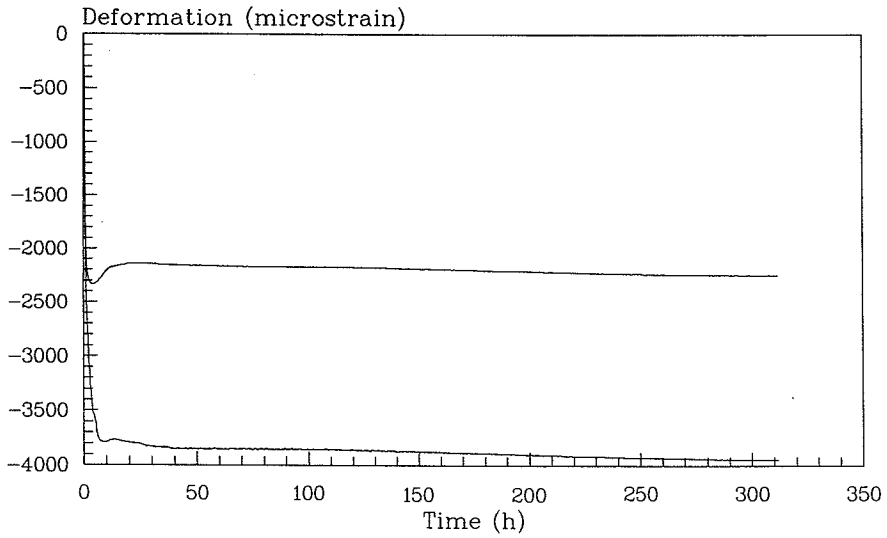

Figure 22. Autogenous deformation of Road Directorate mortar at 20°C. Measurements on two samples are shown. A close-up of the measurements after setting is given in Figure 38.

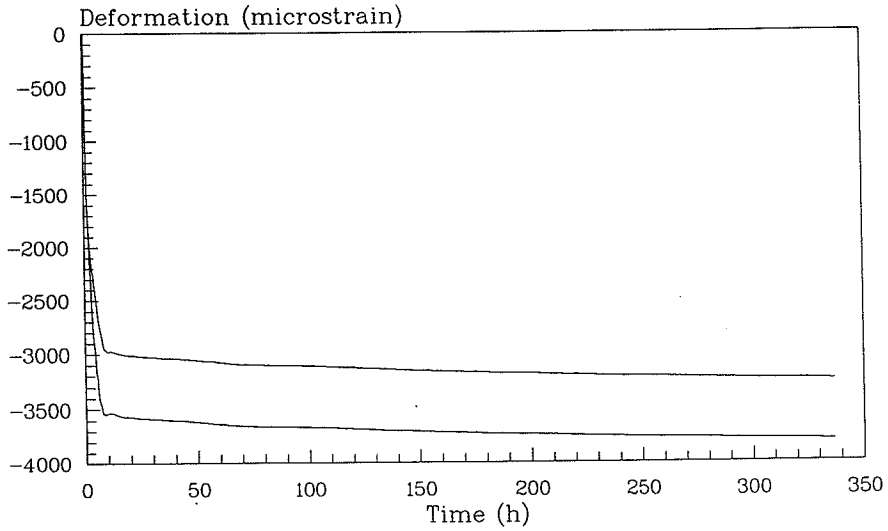

Figure 23. Autogenous deformation of Road Directorate mortar at 40°C. Measurements on two samples are shown. A close-up of the measurements after setting is given in Figure 38.

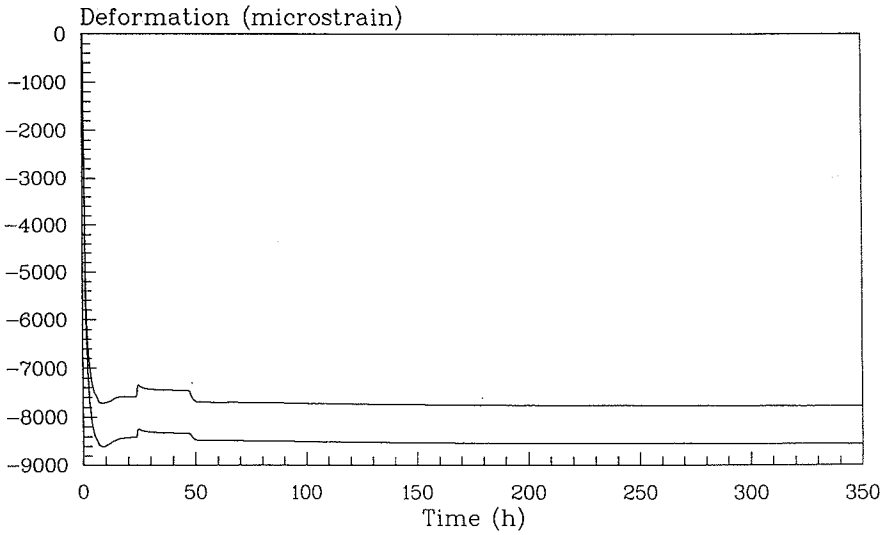

Figure 24. Autogenous deformation of Road Directorate mortar during temperature changes; The temperature is 20°C throughout the experiment except in the period 24 to 48 hours where the temperature is 40°C. Measurements on two samples are shown. A close-up of the measurements after setting is given in Figure 36.

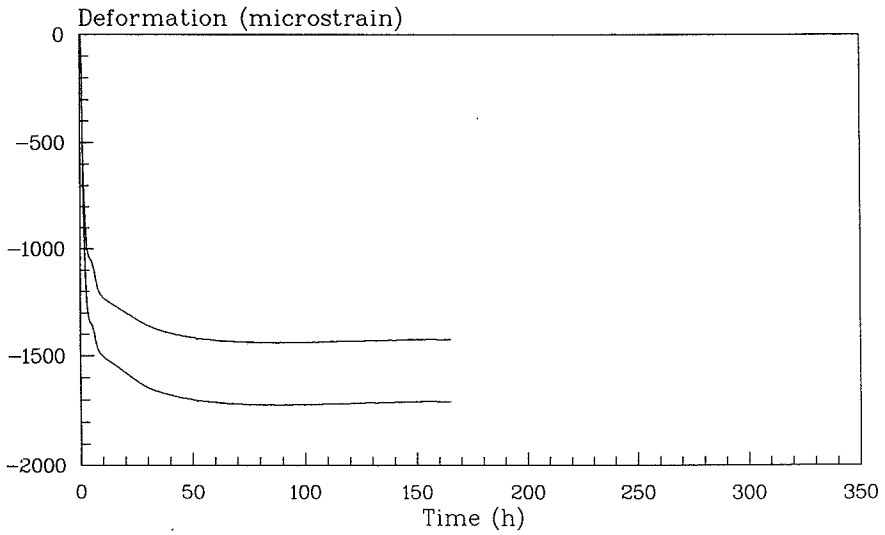

Figure 25. Autogenous deformation of the alternative mortar at 24°C. Measurements on two samples are shown. A close-up of the measurements after setting is given in Figure 39.

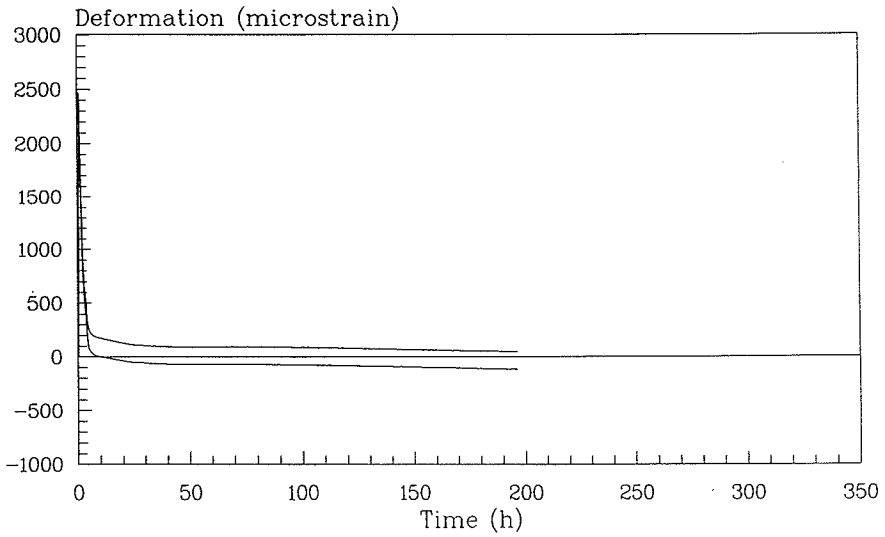

Figure 26. Autogenous deformation of the alternative mortar at 40°C. Measurements on two samples are shown. A close-up of the measurements after setting is given in Figure 39.

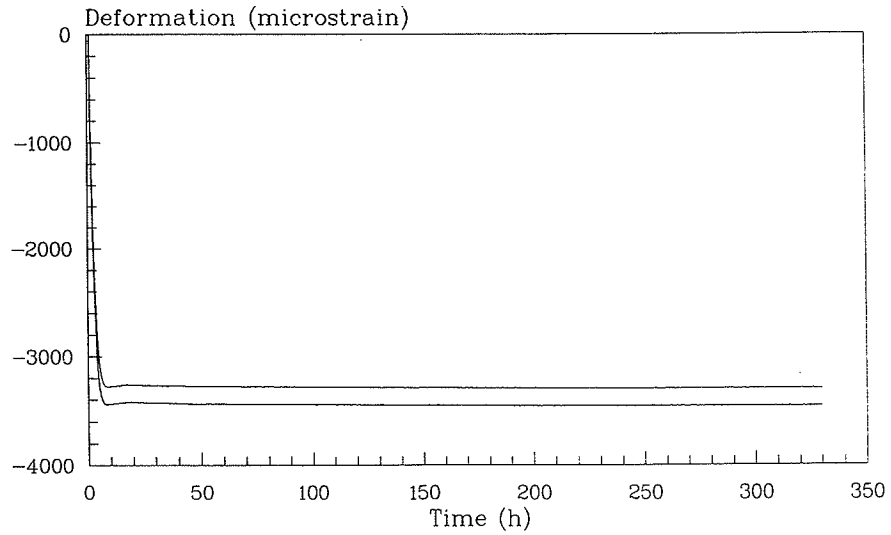

Figure 27. Autogenous deformation of Road Directorate concrete at 24°C. Measurements on two samples are shown. A close-up of the measurements after setting is given in Figure 40.

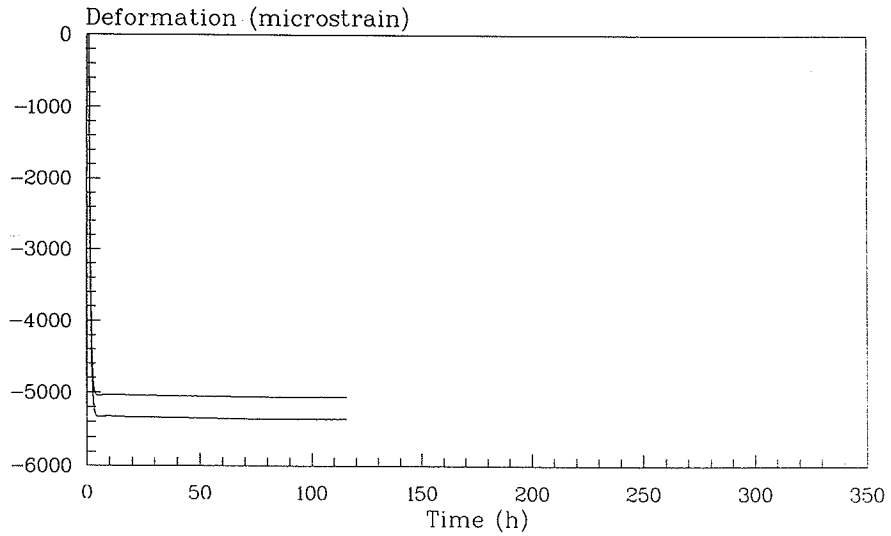

Figure 28. Autogenous deformation of Road Directorate concrete at 40°C. Measurements on two samples are shown. A close-up of the measurements after setting is given in Figure 40.

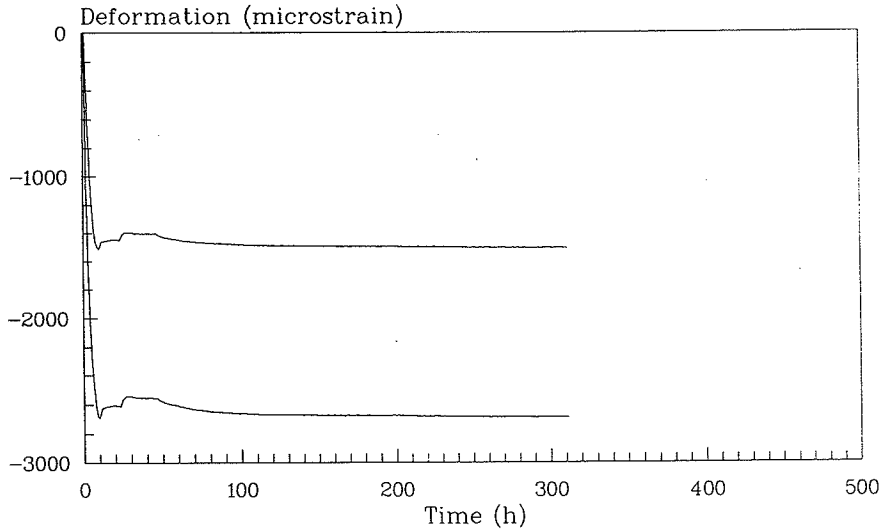

Figure 29. Autogenous deformation of Road Directorate concrete during temperature changes; The temperature is initially 20°C. At 10 hours the temperature is changed to 30°C, at 24 hours to 40°C, and at 48 hours a slow cooling down to 20°C starts. Measurements on two samples are shown.

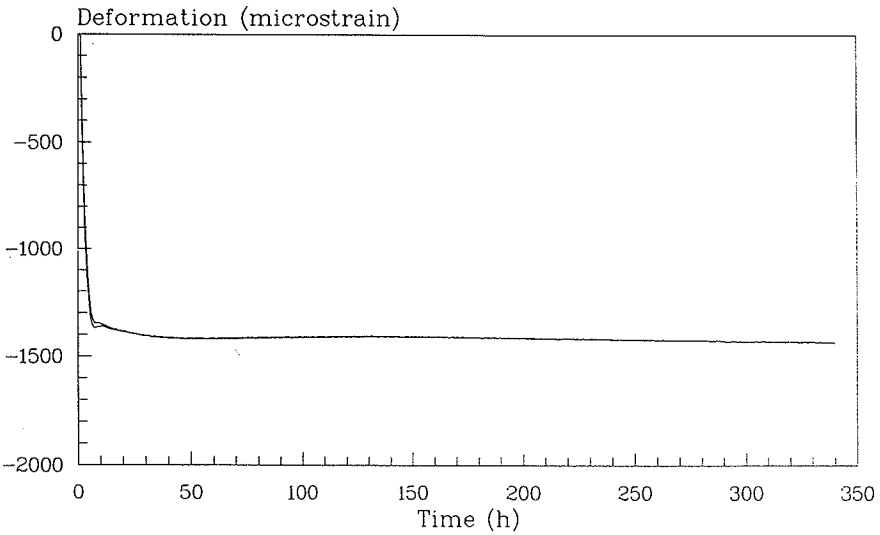

Figure 30. Autogenous deformation of the alternative concrete at 24°C. Measurements on two samples are shown. A close-up of the measurements after setting is given in Figure 41.

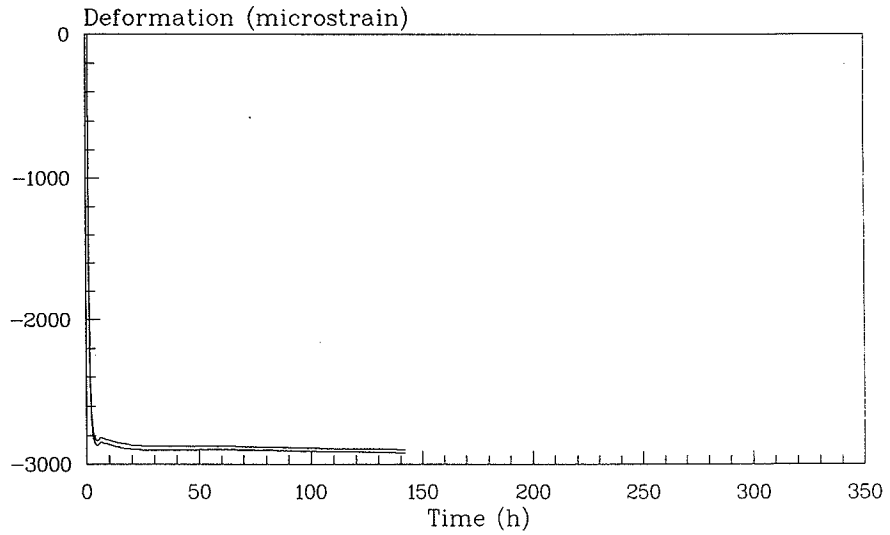

Figure 31. Autogenous deformation of the alternative concrete at 40°C. Measurements on two samples are shown. A close-up of the measurements after setting is given in Figure 41.

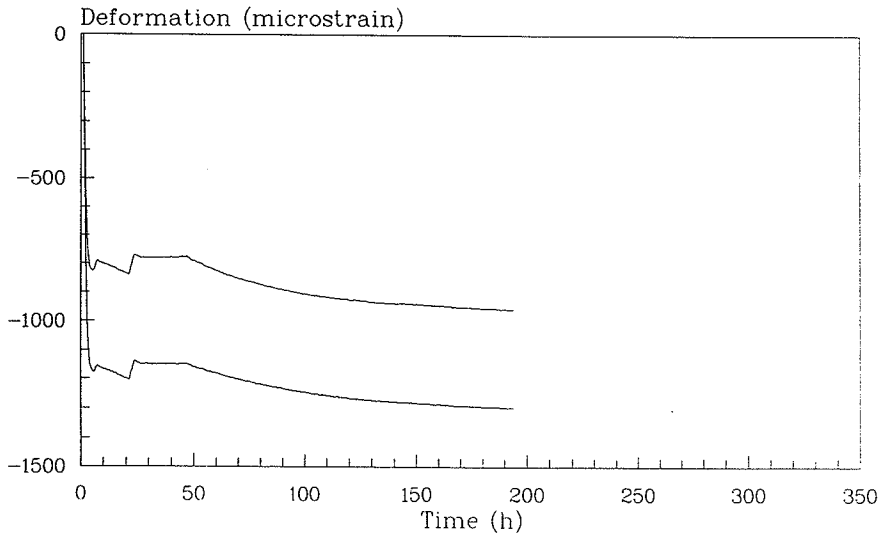

Figure 32. Autogenous deformation of the alternative concrete during temperature changes; The temperature is initially 24°C. At 6 hours the temperature is changed to 30°C, at 22 hours to 40°C, and at 48 hours a slow cooling down to 24°C starts. Measurements on two samples are shown. A close-up of the measurements after setting is given in Figure 37.

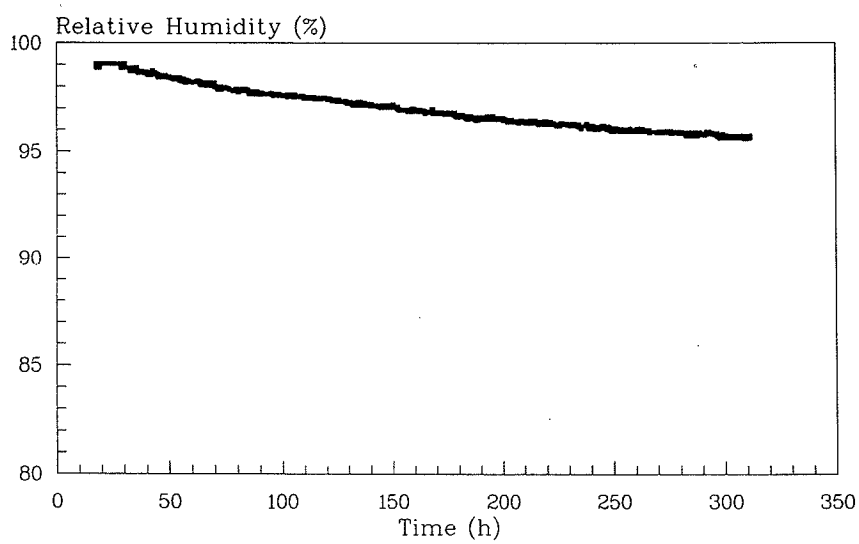

Figure 33. Autogenous RH-change of Road Directorate mortar at 20°C. The curve is an average of four simultaneous measurements.

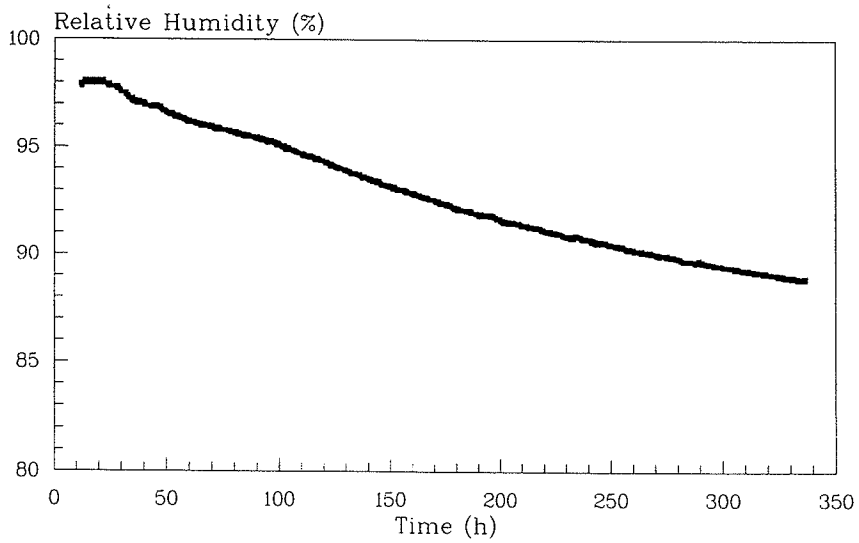

Figure 34. Autogenous RH-change of Road Directorate mortar at 40°C. The curve is an average of four simultaneous measurements.

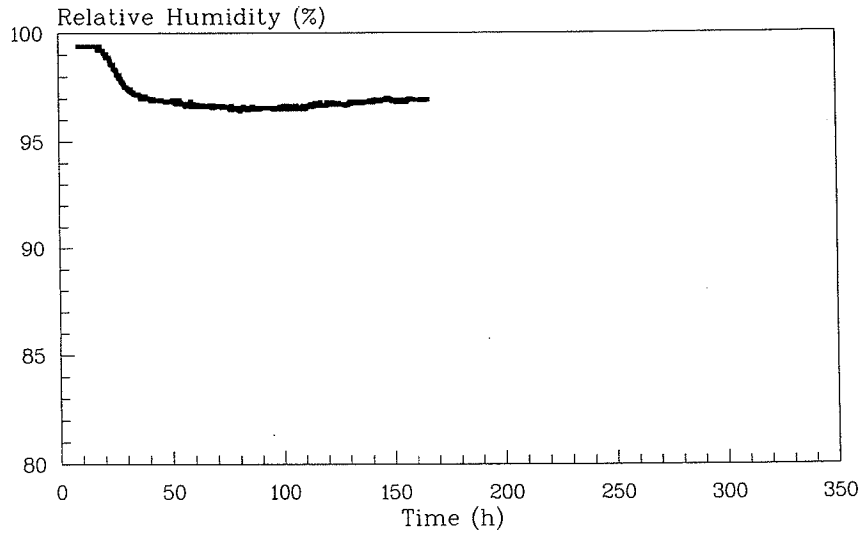

Figure 35. Autogenous RH-change of the alternative mortar at 24°C. The curve is an average of four simultaneous measurements.

6 Discussion

The autogenous deformation histories for the mortars and concretes shown in Figure 22-Figure 32 are the effects of a number of shrinkage and expansion mechanisms.

Setting of the various mixes takes place 5-10 hours after adding water. The deformations registered prior to setting are 10-100 times greater than the deformations after setting. Despite this, cracks do not appear before setting, as the concrete is plastic in this period.

Earlier investigations[1] have shown that the contraction observed prior to setting is caused by the chemical shrinkage involved in the hydration process, which results in an overall shrinkage. If the measurements are carried out at a temperature that involves an initial warming of the materials, e.g. 40° C, expansion can arise due to separation of air from the mixing water and thermal expansion.

Shrinkage and expansion have also been measured in mortar and concrete after setting. Immediately after setting an expansion is observed on several graphs. This expansion is accompanied by a temperature rise in the test specimens due to the heat of hydration. However, the expansion cannot be accounted for by thermal expansion. In concretes, a rise of ½°C in the central temperature has been measured 5-15 hours after the addition of water, whereas the expansion is up to 25 μstrain. The curves shown have not been corrected for temperature deformation, becaurse the development of the coefficient of thermal deformation of the concretes investigated is not known. The coefficient of thermal expansion varies with the degree of hydration. It will normally decline from approx. 20-30 μstrain/°C in the hours around setting[19,1] to approx. 10 μstrain/°C for well-hardened concrete.

In a traditional concrete, autogenous shrinkage after setting is typically[8] 50 to 100 μstrain. For the two concretes shown in Figure 40 and Figure 41, autogenous shrinkages of 30-80 μstrain were registered. This is similar to a traditional concrete.

The measurements of autogenous RH-change shown in Figure 33-Figure 35 harmonize with the deformation measurements. At 20-24°C, the RH was lowered by approx. 3% after one week. This is modest compared with a high-strength concrete, in which an RH-lowering of over 10%[13] can be observed after the same period.

With the given experimental data, it is not possible to connect physical and chemical processes to the registered RH changes and the deformations after setting. On the other hand, the deformation measurements can be used for:

- determination of the coefficient of thermal expansion of the mixes,

□ testing the maturity concept based on Arrhenius transformations,

□ testing the composite theoretical models, and

□ calculating the build-up of stresses, including the evaluation of the risk of cracking during hardening.

This will be carried out in the following and in other reports of the HETEK project.

6.1 Coefficient of thermal expansion

The coefficient of thermal expansion can be estimated based on the measurements shown in Figure 24, Figure 29 and Figure 32.

For the Road directorate concrete the temperature has been changed in the following steps: 20→30°C, 30→40°C and 40→20°C. The temperature change from 40 to 20°C took more than a week due to lack of active cooling. Consequently only the two first temperature changes are used for estimating the coefficient of thermal expansion. In these cases the samples are in thermal equilibrium within 4 hours after the temperature change. The following values were measured for the two samples:
20→30°C: #1: 8.0 μstrain/°C, #2: 6.6 μstrain/°C
30→40°C: #1: 6.2 μstrain/°C, #2: 5.4 μstrain/°C

The coefficient of thermal expansion for the Road Directorate concrete was found to be 7±2 μstrain/°C.

For the alternative concrete the temperature has been changed in the following steps: 24→30°C, 30→40°C and 40→24°C. The temperature change from 40 to 20°C took more than a week due to lack of active cooling. Consequently only the two first temperature changes, 24→30°C and 30→40°C, are used for estimating the coefficient of thermal expansion. The following values were measured for the two samples:
24→30°C: #1: 4.8 μstrain/°C, #2: 6.8 μstrain/°C
30→40°C: #1: 7.4 μstrain/°C, #2: 7.9 μstrain/°C

The coefficient of thermal expansion for the alternative concrete was found to be 7±2 μstrain/°C.

For the mortar the temperature has been changed 20→40→20°C. Due to smaller samples and more effective cooling and heating the temperature change takes less than 1 hour in the case of heating and less than 4 hours for cooling. The following values were measured for the two samples:
20→40°C: #1: 11.2 μstrain/°C, #2: 7.1 μstrain/°C
40→20°C: #1: 12.4 μstrain/°C, #2: 8.9 μstrain/°C

The coefficient of thermal expansion for the Road Directorate mortar was found to be 10±3 μstrain/°C

The measured values are in agreement with values reported in the literature[8]. The coefficient of thermal expansion for the concrete is lower than the value for mortar, probably due to a higher aggregate content, approximately 70% comparred to 40%.

6.2 Activation energy

A single point estimate of the activation energy of autogenous deformation can be made based on measurements at varying temperature. Such measurements for the Road Directorate mortar are shown in Figure 36.

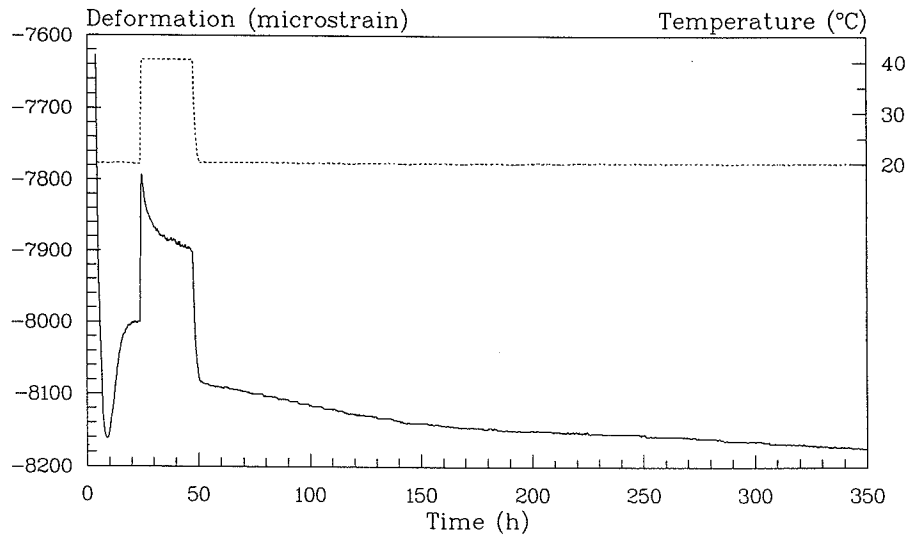

Figure 36. Close-up of autogenous deformation (solid line) of Road Directorate mortar during temperature changes. The graph is an average of the two measurements shown in Figure 24. The temperature (broken line) is 20°C throughout the experiment except from the period 24 to 48 hours where the temperature is 40°C.

From the measurements at a constant temperature it is known that the observed initial expansion (10 to 20 hours in Figure 36) is followed by shrinkage. The temperature change at 24 hours, however seems to trigger off a strong acceleration of the following shrinkage. Therefore, the first temperature change cannot be used for estimating the activation energy.

The change in deformation rate $v_\varepsilon(t,T)$ related to the temperature change at 48 hours is used in the following. By extrapolation it is possible to estimate the deformation rate in a common point for the two temperatures. Numerical differentiation of the measurements in Figure 36 gives: v_ε(48 h, 40°C)=1.5 μstrain/h and v_ε(48 h, 20°C)=0.75 μstrain/h.

From these values the activation energy of autogenous deformation for the Road Directorate mortar can be estimated as[7]:

$$E_a = -\frac{R}{1/T_1 - 1/T_2} \ln\left(\frac{v_{\varepsilon,T_1}}{v_{\varepsilon,T_2}}\right) = -\frac{8.314}{1/313 - 1/293} \ln\left(\frac{1.5}{0.75}\right) = 26 \ \frac{\text{kJ}}{\text{mol}}$$

It must be emphasized that the calculated value is very uncertain and only covers a single point. The maturity concept may be difficult to apply to autogenous deformation and the energy of activation may have no general practicability in the present case[12].

A corresponding calculation for the concretes gives no reasonable results. As seen from Figure 37, the deformation rate is not changed or may even be lowered when the temperature is raised. This corresponds to activation energies equal to or lower than zero.

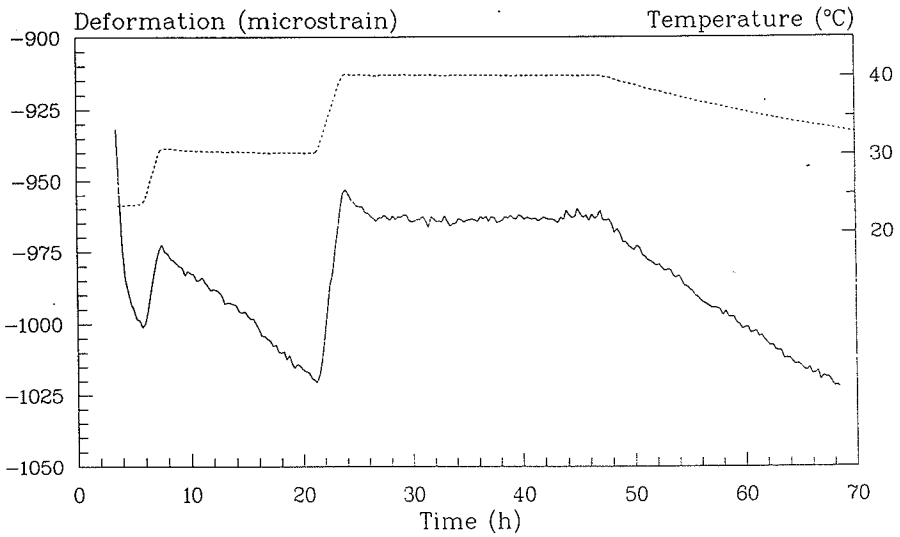

Figure 37. Close-up of autogenous deformation (solid line) of the alternative concrete during temperature changes. The graph is an average of the two measurements shown in Figure 32. The temperature (broken line) is initially 24°C. At 6 hours the temperature is changed to 30°C, at 22 hours to 40°C, and at 48 hours a slow cooling down to 24°C starts.

6.3 Maturity transformation

Maturity transformed and non-transformed autogenous deformation is shown in Figure 38 to Figure 41. The maturity transformation is performed with the Arrhenius function[6]. Since no physical zero-point for the measured deformation exists, the curves have been displaced along the deformation axis for easy comparison.

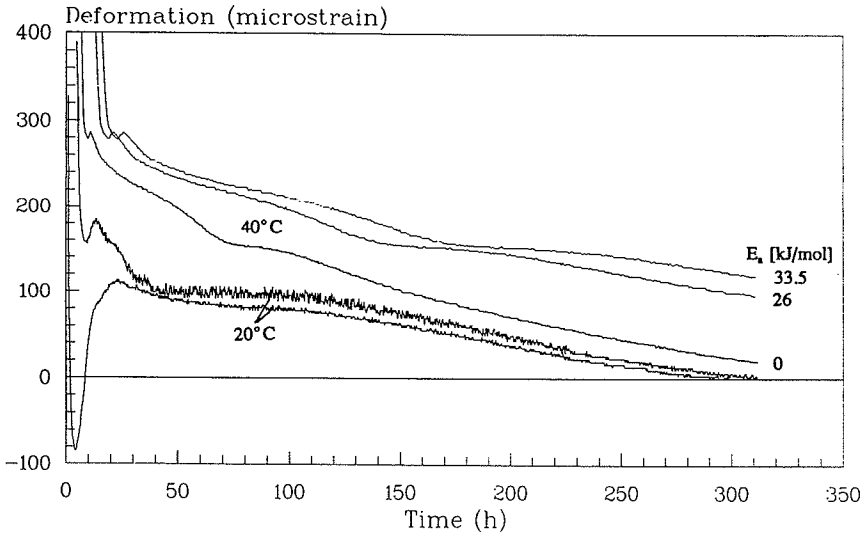

Figure 38. Close-up of autogenous deformation of Road Directorate mortar at 20°C and 40°C. The curves for the two consecutively measured samples at 20°C differ considerably from each other within the first 24 hours; both these are therefore shown. For the 40°C curve an average is shown since the two curves agreed well. Two examples of maturity transformation from 40°C to 20°C are shown: E_a=33.5 and 26 kJ/mol. E_a=0 kJ/mol is the non-transformed curve at 40°C.

Autogenous deformation of Road Directorate mortar is shown in Figure 38. The curves for both test specimens are shown for the 20°C test, as they differ considerably for the first 24 hours. The variation may be due to the composition of the mortar. As mentioned earlier, a great change in the early hardening process takes place if the finest fraction of the sand is removed. Neither of the two 20°C curves in Figure 38 can be excluded in making comparisons with the other curves. The first 24 hours of Figure 36, which is a repetition of this measurement, coincides roughly with the lower 20°C curve in Figure 38. The upper 20°C curve, however, resembles the 40°C curve in Figure 38.

For the 40°C curve, two maturity transformations are shown, corresponding to E_a=33.5 and 26 kJ/mole. E_a=33.5 kJ/mole is traditionally[29] used in concrete technology, while E_a=26 is determined in Section 6.2. Neither of these transformations gives a good description of the history at 20°C. Parts of the 20°C curve are in fact described better by the untransformed 40°C curve, e.g. the period after 150 hours. For the registered autogenous deformation, it appears that a temperature change cannot be simply described by a time-transformation.

This conclusion is further strengthened if the 20°C test and the test with varying temperature, Figure 36, are compared. If the autogenous deformation can be maturity transformed in the traditional way, 24 hours at 40°C (24-48 hours in Figure 36) will solely involve a time-shift of about 35 hours relative to the 20°C curve. This means that the curve after approx. 48 hours in Figure 36 should be

identical with the 20°C curve in Figure 38 after approx. 83 hours. This is not the case: That part of the curve in Figure 36 is concave upwards, while the corresponding part of the curve in Figure 38 is mainly concave downwards.

Neither can the influence of temperature on the autogenous deformation of the alternative mortar be simply described by a time-transformation, see Figure 39. Especially in the period 10-50 hours, there is a considerable difference in the shrinkage at 20° and 40°C. Furthermore, the observed expansion after 80 hours at 20°C cannot be found at 40°C.

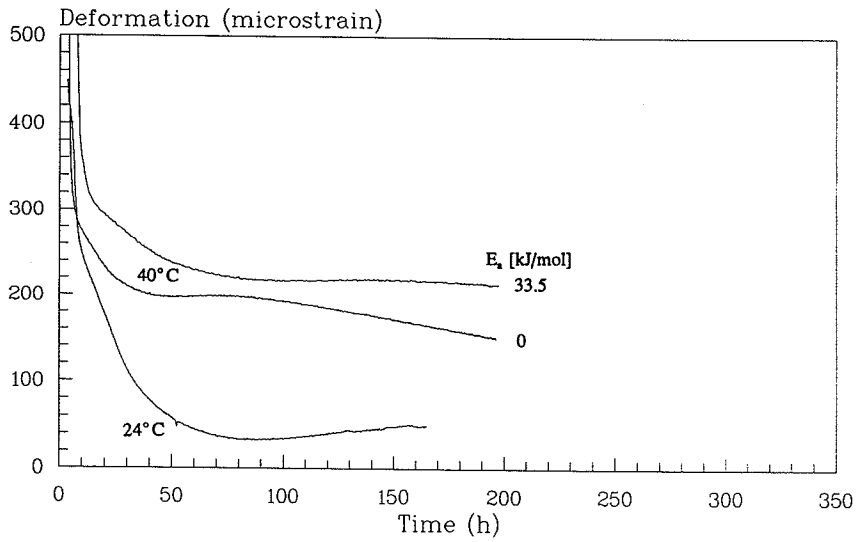

Figure 39. Close-up of autogenous deformation of the alternative mortar at 24°C and 40°C. Each curve is an average of measurements on two samples. A maturity transformation from the 40°C graph to 24°C is shown: E_a=33.5 kJ/mol. E_a=0 kJ/mol is the non-transformed curve at 40°C.

Curves for the autogenous deformation of the Road Directorate concrete are shown in Figure 40. The maturity-transformed 40°C curve is a much better description of the 24°C history than the untransformed curve. However, the expansion after setting is twice as large at 24°C as at 40°C. A maturity transformation does not change the magnitude of the deformation. Furthermore, the rate of shrinkage declines more rapidly for the transformed 40°C curve than the 24°. The deformations in this concrete after setting are modest - approx. 30-40 μstrain. The difference between the transformed 40°C curve and the 24°C curve may therefore be due to measurement uncertainty.

Curves for autogenous deformation of the alternative concrete are shown in Figure 41. As for the Road Directorate concrete, the maturity-transformed 40°C curve is a better description of the 24°C history than the untransformed curve. However, the 40°C curve shows an expansion of approx. 20 μstrain immediately after setting, which does not take place at 24°C. Also, the 24°C curve shows an expansion in the 50-150 hours interval, which does not appear at 40°C.

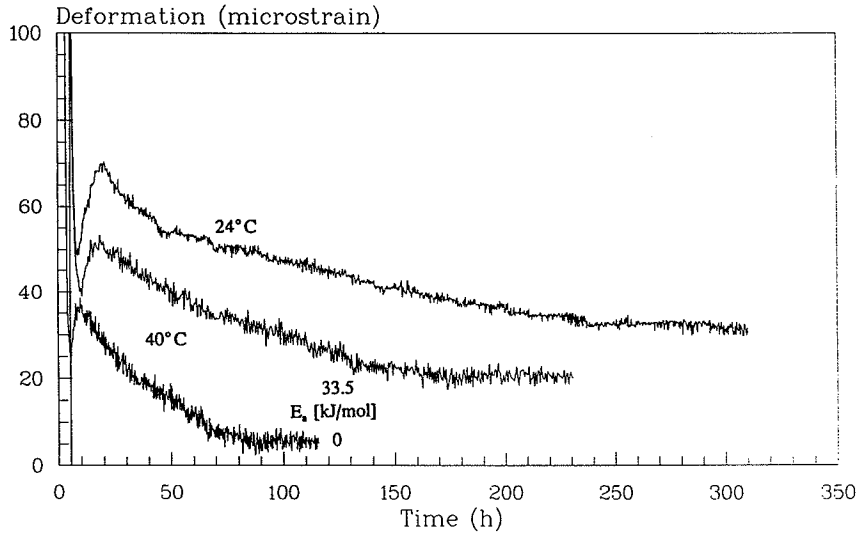

Figure 40. Close-up of autogenous deformation of the Road Directorate concrete at 24°C and 40°C. Each curve is an average of measurements on two samples. A maturity transformation from the 40°C graph to 24°C is shown: E_a=33.5 kJ/mol. E_a=0 kJ/mol is the non-transformed curve at 40°C.

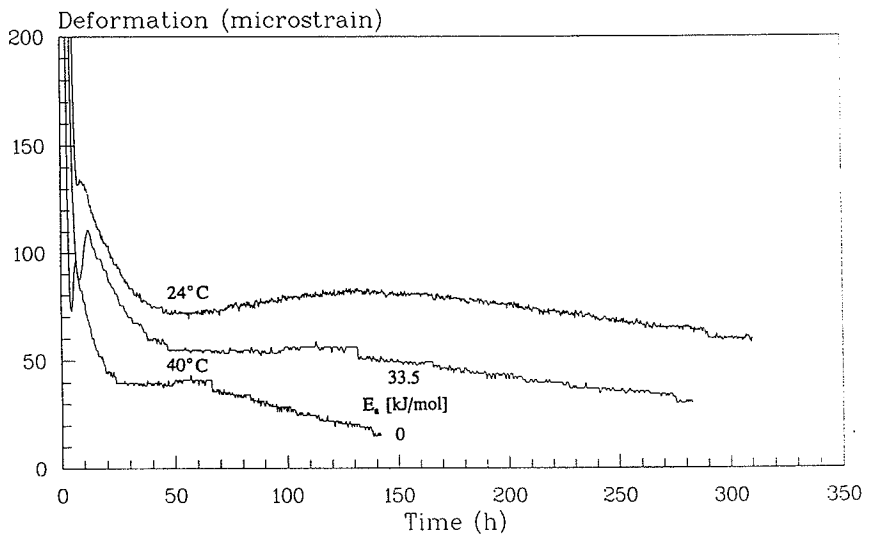

Figure 41. Close-up of autogenous deformation of the alternative concrete at 24°C and 40°C. Each curve is an average of measurements on two samples. A maturity transformation from the 40°C graph to 24°C is shown: E_a=33.5 kJ/mol. E_a=0 kJ/mol is the non-transformed curve at 40°C.

7 Conclusion

This report describes fundamental knowledge about autogenous deformation and autogenous change of the relative humidity in hardening cement paste systems. Furthermore, a series of measurements of autogenous deformation and autogenous RH-change of a structural concrete used by the Danish Road Directorate and of a concrete with an alternative mix is reported. The mortars of the two concretes were also investigated.

The measured autogenous RH-change amounted to a few percent. The associated shrinkage was 100-200 μstrain for the mortars and 30-80 μstrain for the concretes. This is similar to traditional concretes.

On the basis of the measurements carried out under the present project, it is not possible to give a clear answer to the question of whether the traditional maturity concept is applicable to autogenous deformation. For the Road Directorate mortar, the activation energy for autogenous deformation at a certain degree of hydration was found to be 26 kJ/mol. Maturity transformation of measurements with this value do not, however, give a satisfactory account of the influence of temperature.

The coefficient of thermal expansion was determined for the 20-40°C interval by means of a dilatometer. The coefficient was found to be 10±3 μstrain/°C for the mortars, and 7±2 μstrain/°C for the concretes.

Symbols

SYMBOL	NAME	SI-UNIT
C	molar concentration	mol/l
E_a	activation energy	J/(mol·K)
M	molar mass	kg/mol
n	number of moles	[]
p	stress	Pa
p_s	vapour pressure of water-saturated air	Pa
r	radius	m
R	gas constant, 8.314	J/(mol·K)
RH	relative humidity	[]
S	specific surface	m^2/kg
T	absolute temperature	K
u	moisture content	kg/kg
V	molar volume	m^3/mol
v_ε	deformation rate	strain/h
V	volumetric fraction	[]
w/c	water-cement ratio	kg/kg
X	molar fraction	mol/mol
α	degree of hydration	[]
Δ	change	
ε	strain	[]
θ	contact angle	°
ρ	density	kg/m^3
σ	surface tension	N/m

INDEX

a	anhydrate
c.w	capillary water
ce	cement
g	gas
g.s	gel solid
g.w	gel water
h	hydrate
hydr	hydration
kryst	crystal
l	liquid, linear
osm	osmotic
p	pores
s	salt, self-desiccation, solid, saturated
w	water

The usual cement-technological nomenclature for oxides is used: C=CaO, S=SiO_2, H=H_2O, A=Al_2O_3, F=Fe_2O_3 osv.

Literature

1. O. Mejlhede Jensen: "Autogenous deformation and change of the relative humidity - self-desiccation and self-desiccation shrinkage" (in Danish), Technical Report 284/93, Building Mat. Lab., Techn. Univ. Denmark, 1993

2. R L'Hermite, J-J Grieu: "Études expérimentales récentes sur le retrait des ciments et des bétons", Annales de l'institut technique du batiment et des travaux publics, 52-53, p 491-514, 1952

3. W Czernin: "Über die Schrumpfung des erhärtenden Zementes", Zement-Kalk-Gips, 12, p 525-530, 1956

4. M del Campo: "A new method to study the early volume changes on the neat cement paste", Rilem bulletin, 4, p 18-23, 1959

5. F O Slate, R E Matheus: "Volume Changes on Setting and Curing of Cement Paste an Concrete from Zero to Seven Days", ACI Journal (Journal of the American Concrete Institute), 1, p 34-39, 1967

6. P Freiesleben Hansen and E J Pedersen: "Måleinstrument til kontrol af betons hærdning", Nordisk Betong, pp. 21-25, 1977

7. O Mejlhede Jensen: "Svind af fiberaremeret cementmørtel", FYM, DIA-B, 1988

8. A M Neville and J J Brooks: "Concrete Technology", Longman Scientific & Technical, Essex, 1987

9. N Setter, D M Roy: "Mechanical features of chemical shrinkage of cement paste", Cement and concrete research, 8, p 623-634, 1978

10. O Mejlhede Jensen: "Rotronic Hygroskop DT Fugtmåleudstyr - kalibrering og afprøvning", Laboratoriet for Bygningsmaterialer, DtH, Teknisk rapport 282/93, 1993

11. O Mejlhede Jensen and P Freiesleben Hansen: "A dilatometer for measuring autogenous deformation in hardening Portland cement paste", Materials and Structures, vol. 27, pp. 406-409, 1995

12. O Mejlhede Jensen: "Notes on the maturity concept of autogenous deformation", Seminar on early volume change and reactions in paste - mortar - concrete, NTNU, Trondheim, November 1996

13. O Mejlhede Jensen and P Freiesleben Hansen: "Autogenous relative humidity change in silica fume-modified cement paste", Advances in Cement Research, vol. 7, No. 25, pp. 33-38, 1995

14. G D de Haas, P C Kreijger, E M M G Niël, J C Slagter, H N Stein, E M Theissing, M van Wallendael: "The shrinkage of hardening cement paste and mortar", Cement and concrete research, 5, p 295-320, 1975

15. O Mejlhede Jensen and P Freiesleben Hansen: "Autogenous deformation and change of the relative humidity in silica fume modified cement paste", ACI Materials Journal, Nov-Dec issue, 1996

16. P Rossi, N Godart, J L Robert, J P Gervais and D Bruhat: "Investigation of basic creep of concrete by acoustic emmision", Materials and Structures, Vol. 27, pp. 510-514, 1994

17. E Tazawa, Y Matsuoka, S Miyazawa and S Okamoto: "Effect of autogenous shrinakge of self stress in hardening concrete", RILEM International Symposium on Thermal Cracking in Concrete at Early Ages, Munic, Oct. 10-12, pp. 221-228, 1994

18. C Hua, P Acker and A. Ehrlacher: "Analuses and models of the autogenous shrinkage of hardening cement paste, I. Modelling at macroscopic scale", Cement and Concrete Research, Vol. 25, No. 7, pp. 1457-1468, 1995

19. P Laplante and C Boulay: "Evolution du coefficient de dilatation thermique du béton en fonction de sa maturité aux tout premiers âges", Materials and Structures, Vol. 27, pp. 596-605, 1994

20. J Baron, M Buil: "Remarques a propos de l'article "Mechanical features of chemical shrinkage of cement paste"", Cement and concrete research, 9, p 545-547, 1979

21. H E Davis: "Autogenous volume changes of concrete", American society for testing materials, ASTM, proceedings 32, 40, p 1103-1112, 1940

22. L E Copeland, R H Bragg: "Self Desiccation in Portland Cement Pastes", Research and Development Laboratories of the Portland Cement Association, PCA Bulletin 52, 1955

23. RILEM commission 42-CEA: "Properties of set concrete at early ages (state of the art report)", Matériaux et constructions, 84, p 426-449, 1981

24. P W Atkins (ed.): "Physical Chemistry, 3 ed.", Oxford University Press, 1988

25. T C Powers: "A Hypothesis on Carbonation Shrinkage", Research Laboratories of the Portland Cement Association, PCA Bulletin 146, 1962

26. M Buil: "Contribution a l'étude du retrait de la pâte de ciment durcissante", Rapport de recherche des Laboratoire Central des Ponts et Chaussées (LPC), 92, 1979

27. O M Jensen: "Mikrosilicas puzzolane reaktion", Laboratoriet for Bygningsmaterialer, DtH, Teknisk rapport 229/90, 1990

28. E J Sellevold, D H Bager, E K Jensen, T Knudsen: "Silica fume - cement pastes: hydration and pore structure", Norwegian Institute of Technology, Trondheim, Report BML 82.610, p 19-50, 1982

29. A D Herholdt, C F P Justesen, P Nepper-Christensen, A Nielsen (ed.): "Beton-Bogen", Aalborg Portland, Cementfabrikkernes tekniske Oplysningskontor, 2 udg., 1985

30. R H Mills: "Factors Influencing Cessation of Hydration in Water Cured Cement Pastes", Highway Research Board, Special Report 90, Symposium on structure of portland cement paste and concrete, p 406-424, 1966

31. M Geiker: "Studies of Portland Cement Hydration", Danmarks tekniske Højskole, Instituttet for Mineralindustri, 1983

32. E Hagemann: "Byggematerialer", Polyteknisk Forlag, 3. udg., 1981

33. E M Winkler, E J Wilhelm: "Salt burst by hydration pressures in architectural stone in urban atmosphere", Geological Society of America Bulletin, 81, p 567-572, 1970

34. C W Correns: "Growth and dissolution of crystals under linear pressure", Discussions of the Faraday Society, 5, p 267-271, 1949

35. E M Winkler: "Stone: Porperties, Durability in Man's Environment", Applied Mineralogy, 4, Springer-Verlag 1973, p 113-125

36. T C Powers, T L Brownyard: "Studies of the Physical Properties of Hardened Portland Cement Paste", Research Laboratories of the Portland Cement Association, PCA Bulletin 22, 1948

37. T C Powers: "Mechanisms of shrinkage and reversible creep of hardened cement paste", Conference on the structure of concrete, London, p 319-344, 1965

38. P McGrath, R D Hooton: "Self-desiccation of portland cement and silica fume modified mortars", Ceramic transactions, Advances in cementitious materials, vol 16, The American ceramic society, p 489-500, 1990

39. I Soroka: "Portland cement paste and concrete", Macmillan press ltd, 1979

40. F de Larrard and R le Roy: "The influence of mix composition on mechanical properties of high-performance silica-fume concrete", Proceedings of the fourth international conference on Fly Ash, Silica Fume, Slag, and Natural Pozzolans in Concrete, pp. 965-986, Istanbul, Turkey, May 1992

41. B G Linsen: "Physical and Chemical Aspects of Adsorbents and Catalysts", Academic Press, London 1970

42. F Henkel: "Zum Kristallisationsdruck betonzerstörender Sulfate", Zement und Beton, 85-86, p 26-28, 1975

43. W Eitel: "Silicate Science, vol. II", Academic Press, London 1965

44. H Weigler, S Karl: "Junger Beton, Teil 1", Betonwerk und Fertigteil-technik, p 392-401, 1974

45. H Garrecht, H K Hilsdorf, J Kropp: "Hygroscopic salts - influence on the moisture behaviour of structual elements", Durability of Building Materials and components, Conference, Nov. 1990, Chapman and Hall, London 1991

46. P F Hansen, O M Jensen: "Selfdesiccation shrinkage in low porosity cement-silica mortar", Nordic Concrete Research, 1989, p 89-102

47. S J Gregg, K S W Sing: "Adsorption, Surface area and Porosity", Academic Press, 2. ed., London 1982

48. H Lund: "Uorganisk kemi", Gads forlag, 3. udg., København 1959

49. R C Weast (ed.): "Handbook of Chemistry and Physics", Chemical Rubber Compagny, 1984

50. H Justnes, E J Sellevold, G Lundevall: "High Strength Concrete Binders. Part A: Reactivity and Composition of Cement Pastes with and without Condensed Silica Fume", ACI, CANMET
IV International Conference on Fly Ash, Silica Fume, Slag and Natural Pozzoland in Concrete. Istanbul, May 1992

51. E J Sellevold, H Justnes: "High Strength Concrete Binders. Part B: Nonevaporable vater, self-dessication and porosity of cement pastes with and without condensed silica fume", ACI, CANMET, IV International Conference on Fly Ash, Silica Fume, Slag and Natural Pozzoland in Concrete. Istanbul, May 1992

52. A M Paillère, M Buil, J J Serrano: "Effect of Fiber Addition on the Autogenous Shrinkage of Silica Fume Concrete", ACI Materials Journal, March-April 1989, p 139-144

53. E Atlassi: "Influence of cement type on the desorption isotherm of mortar", Nordic concrete research, 10, p 25-36, 1991

54. S Diamond: "A critical comparison of mercury porosimetry and capillary condensation pore size distributions of portland cement pastes", Cement and concrete research, 1, p 531-545, 1971

55. L Brüll, K Komlos: "Early volume changes of cement pastes and cement mortars", International conference on concrete of early ages, RILEM, Paris 1982, p 29-34

56. T C Powers: "A discussion of cement hydration in relation to the curing of concrete", Proceedings of the Highway Research Board, 27, p 178-188, 1947

57. G Hedenblad: "Inverkan av salt på jämtviktsisotermen", Avdelingen för byggnadsmateriallära, Tekniska högskolan i Lund, Rapport TVBM-3031, 1987

58. B Persson: "Högpresterande betong en match för management", Byggforskning 6, p 26-27, 1990

59. B Persson: "Höghållfast betong - självuttorkning och hållfasthet", Bygg & teknik 7, p 21-25, 1991

60. M Auperin: "Shrinkage and creep in certain high performance concrete for use on site", Research department Bouygues, 1989

61. G R Gause, J Tucker: "Method for determining the moisture condition in hardened concrete", Journal of research of the national bureau of standards, vol 25, oktober 1940, p 403-416

62. J E McDonald: "Properties of Silica-Fume Concrete. Repair, Evaluation, Maintenance, and Rehabilitation Research Program", AD-A235 369/6/XAD NTIS Issue 9118, Army Engineer Waterways Experiment Station, Structures Lab., Vicksburg, 1991

63. N Gottlieb, M Knudsen: "Selvudtørringssvind i mørtel og beton", Laboratoriet for bygningsmaterialer, DtH, 1991

64. A K Christoffersen, T B Sørensen: "Selvudtørring og kemisk svind i mørtel", Laboratoriet for Bygningsmaterialer, Teknisk rapport 158/86, DtH, 1986

65. F Kortsen, J Tellefsen: "Selvudtørring og kemisk svind", Sektion for fysik og materialer, DIA-B, 1986

66. J C Yates: "Effect of calcium chloride on readings of a volumeter inclosing portland cement pastes and on linear changes of concrete", Highway Research Board, proceedings, vol. 21, p 294-204, 1941

67. C L Page, Ø Vennesland: "Pore solution composition and chloride binding capacity of silica-fume cement pastes", Materials and Structures, vol 16, nr 91, p 19-25, 1983

68. A K Christoffersen, T B Sørensen, A Nielsen: "Selvudtørring af beton", Dansk beton, nr. 4, 1988, p 12-17

69. B Persson: "Högpresterande betong ger fuktsäker platta på mark", Betong, nr. 1, Mars 1991, p 8-10

70. S Ziegeldorf, H S Müller, J Plöhn, H K Hilsdorf: "Autogenous shrinkage and crack formation in young concrete", International conference on concrete of early ages, RILEM, vol 1, p 83-88, 1982

71. L-O Nielsson: "Desoption isotherms for silica-fume/cement mortars", Institute of Moisture Issues in Material and Building Technology, Trelleborg, Sweden, Report IF 8431, 1984

72. X Wei, F P Glasser: "The role of microsilica in the alkali-aggregate reaction", Advances in Cement Research, 2, nr 8, oktober, p 159-169, 1989

73. C E Wuerpel: "Laboratory Studies of Concrete Containing Air-Entraining Admixtures", Journal of the American Concrete Institute (ACI), vol 17 nr 4, februar 1946, p 305-359